Article:
Salisbury, DJ, Brooks, IM and Anguelova, MD (2013) On the variability of whitecap fraction using satellite-based observations. Journal of Geophysical Research C: Oceans, 118 (11). 6201 - 6222. ISSN: 0148-0227

https://doi.org/10.1002/2013JC008797

JOURNAL OF GEOPHYSICAL RESEARCH: OCEANS, VOL. 118, 1–22, doi:10.1002/2013JC008797, 2013

On the variability of whitecap fraction using satellite-based observations

Dominic J. Salisbury,[1] Magdalena D. Anguelova,[2] and Ian M. Brooks[1]

Received 29 January 2013; revised 9 October 2013; accepted 11 October 2013.

[1] Despite decades of effort to accurately quantify whitecap fraction W using in situ photography of the ocean surface, there remains significant scatter in estimates for any given 10 m wind speed (U_{10}). It is believed that the resulting, commonly used, $W(U_{10})$ parameterizations do not fully account for the true variability in W, by failing to incorporate the impact of the wavefield and other environmental conditions. This paper attests to the variability in whitecap fraction attributed to these additional factors, by analyzing satellite-derived W estimates over the globe for a full year. A comparison is made between the wind speed dependence of satellite estimates and three $W(U_{10})$ relationships formulated from in situ photographic data. The influence of various secondary factors on W is investigated once the dominant wind speed dependence is accounted for. The W retrieval's sensitivity to secondary forcings is dependent upon microwave frequency; at 37 GHz it varies by up to 25% of the mean at a given wind speed, while at 10 GHz it is a maximum of 8%. This results from a frequency-dependent sensitivity to foam depth; at 10 GHz predominantly foam from active breaking waves is detected, while at 37 GHz thin foam in residual whitecaps is also seen. Principal component analysis is used to rank variables by their success in accounting for variability in W. After wind speed, the most important secondary factor that accounts for variability in W is the wavefield. A wind-wave Reynolds number accounts for almost as much variability in W as wind speed.

Citation: Salisbury, D. J., M. D. Anguelova, and I. M. Brooks (2013), On the variability of whitecap fraction using satellite-based observations, *J. Geophys. Res. Oceans*, *118*, doi:10.1002/2013JC008797.

1. Introduction

[2] Oceanic whitecaps are an important but still poorly understood feature of the wind-driven sea [*Massel*, 2007]. Whitecaps form when breaking waves entrain air into the seawater forming clouds of bubbles, which subsequently rise to the surface and form patches of foam. The characteristic whiteness of sea foam is due to light scattering through the air-water mixture. The fraction of the ocean surface covered in sea foam is known as the whitecap fraction W, with the global average estimated to be 1–4% [*Blanchard*, 1963, 1983]. Although wave breaking and whitecap formation are controlled to first order by the wind, a number of factors influence how ocean waves form, develop, break, and dissipate part of their energy through formation of whitecaps.

[3] A variety of physical and chemical processes are affected by breaking waves and whitecaps at the air-sea interface, including the exchange of momentum and heat [*Andreas and Monahan*, 2000; *Fairall et al*., 2003]. Bubble entrainment by breaking waves provides an efficient mechanism for the exchange of gases, thus enhancing the total air-sea transfer [*Woolf*, 1997; *Wanninkhof et al*., 2009]; it has been argued that the bubble-mediated contribution should scale with W [*Monahan and Spillane*, 1984; *Woolf*, 2005]. Whitecaps are areas where sea spray droplets are actively produced through bubble bursting, and via the wind tearing of wave crests at higher wind speeds [*Blanchard*, 1963; *Monahan et al*., 1983; *Andreas*, 1995]. Recently, the importance of wave breaking and whitecap formation in the transfer of organic matter from the ocean surface into the atmosphere has been increasingly recognized [e.g., *Monahan and Dam*, 2001; *O'Dowd et al*., 2004, 2008; *Vignati et al*., 2010; *de Leeuw et al*., 2011]. Upon injection into the lower atmosphere, spray droplets can play a variety of roles depending upon their size. Smaller droplets ($r \leq 1$ μm), having a residence times of the order of days, play a vital role in the climate system both directly through the scattering of solar radiation [*Haywood et al*., 1999], and indirectly by acting as cloud condensation nuclei, and thus affecting cloud albedo [*Andreae and Rosenfeld*, 2008]. Larger droplets ($r \geq 25$ μm), despite having short residence times of the order of seconds, can affect interfacial fluxes of sensible and latent heat at high wind speeds [*Andreas et al*., 1995, 2008], and are believed to affect the intensity of tropical cyclones [*Andreas and Emanuel*, 2001].

[1]Institute for Climate and Atmospheric Science, University of Leeds, Leeds, UK.
[2]Remote Sensing Division, Naval Research Laboratory, Washington, District of Columbia, USA.

Corresponding author: D. J. Salisbury, Institute for Climate and Atmospheric Science, University of Leeds, West Yorkshire, Leeds LS2 9JT, UK. (eedjs@leeds.ac.uk)

2169-9275/13/10.1002/2013JC008797

[4] The presence of whitecaps increases ocean albedo [*Koepke*, 1984] and thus must be accounted for in models of the global radiation budget [*Frouin et al*., 2001]. Consideration of whitecaps is also required in optical ocean color retrievals due to the masking of water-leaving radiance by foam patches [*Gordon and Wang*, 1994]. At microwave frequencies, whitecaps are areas with increased surface emission and brightness temperature [*Wentz*, 1983; *Smith*, 1988; *Rose et al*., 2002]. This has implications for many remote sensing applications, including the use of satellite-borne radiometers to obtain the surface wind vector [*Wentz*, 1997; *Yueh*, 1997; *Gaiser et al*., 2004].

[5] An accurate parameterization of whitecap fraction is a requirement for successful modeling of whitecap-dependent processes. In nearly all current geophysical models, whitecap fraction is specified as a simple function of wind speed, $W(U_{10})$, where U_{10} is the wind speed at a 10 m reference height. As such, a reliable estimate of W is only obtained if it is assumed that wind speed can fully predict whitecap fraction; however, there is substantial evidence that this is not the case [*Monahan and O'Muircheartaigh*, 1986; *Anguelova and Webster*, 2006; *Callaghan et al*., 2008b].

[6] Here we present an analysis of the variability of whitecap fraction using satellite-derived estimates of W. In section 2, we summarize relevant background information and outline the need for a comprehensive database of W measurements in the light of the limitations of using in situ data. Section 3 describes the data used in this study, the calculation of additional factors influencing whitecap fraction, and the analyses used. In section 4, we explore the wind speed dependence of satellite-derived W, investigate the dependence of W on various factors, and quantify how important each variable is in accounting for variability in W. We follow with a discussion of our findings (section 5), and conclusions (section 6), regarding the variability of whitecap fraction and the utility of satellite-derived estimates of W for future direct monitoring and quantifying of this variability.

2. Whitecap Observations

2.1. Traditional Measurement of Whitecap Fraction

[7] Estimates of whitecap fraction have traditionally been obtained from in situ measurement of the ocean surface via photographic or video imagery [*Lewis and Schwartz*, 2004; *Anguelova and Webster*, 2006; *de Leeuw et al*., 2011]. Measurements have been made from aircraft [e.g., *Bobak et al*., 2011; *Kleiss and Melville*, 2011], ships [e.g., *Callaghan et al*., 2008a], and fixed platforms [e.g., *Callaghan et al*., 2008b; *Sugihara et al*., 2007]. *Anguelova and Webster* [2006] give a chronological listing of whitecap fraction data sets spanning nearly 50 years, from 1952 to 2000. There exists large variation in estimates of whitecap fraction, spanning several orders of magnitude. Part of this variation is likely due to differences in both whitecap observation methods and wind speed measurement methods. Furthermore, conditions encountered between different measurement campaigns also show large variation, yet often there is not sufficient documentation of environmental conditions (such as sea surface temperature, air-sea stability, and wave state) to make a reliable comparison between data sets.

2.2. Previous Wind Speed Parameterizations of Whitecap Fraction

[8] Wind speed is the first-order controlling factor for wave breaking and the formation of whitecaps, and being routinely measured, is often used to parameterize whitecap fraction through an empirical expression, $W = f(U_{10})$. Nearly all of these relationships are expressed as a power law of the form aU_{10}^b with the exponent b typically close to three [*Anguelova and Webster*, 2006]. A cubic relationship between W and a wind parameter (either wind speed or friction velocity, u_*) has a strong theoretical grounding: *Cardone* [1969] hypothesized that W, related to energy dissipation through wave breaking, should be directly related to the rate of energy transferred to the wavefield through the action of the wind. *Wu* [1988] determined this on dimensional grounds by noting that W should be proportional to the energy flux supplied by the wind, which is itself proportional to the cube of the turbulent friction velocity.

[9] As numerous parameterizations exist within the literature, it is often a matter of preference as to which formulation should be utilized. Despite being one of the earliest formulations, the *Monahan and O'Muircheartaigh* [1980] relationship, obtained using the robust biweight fitting technique on a combination of field data reported in *Monahan* [1971] and *Toba and Chaen* [1973], has been widely adopted in the parameterization of sea spray aerosol production in models:

$$W(U_{10}) = 3.84 \times 10^{-4} U_{10}^{3.41}, \tag{1}$$

where W is in %. The highest wind speed recorded in the combined data set is 16.6 m s^{-1}, but a maximum wind speed above which (1) is no longer suitable, is not explicitly defined.

[10] The *Callaghan et al*. [2008a] relationship is a recent formulation resulting from analysis of whitecap data obtained during the 2006 Marine Aerosol Production (MAP) campaign in the North East Atlantic. By assuming that W can be related to U_{10} with a power law of the form $W = a(U_{10} + b)^3$, a linear regression on $W^{1/3}$ against U_{10} was performed, resulting in the following relationships:

$$\begin{aligned} W(U_{10}) &= 3.18 \times 10^{-3}(U_{10} - 3.70)^3; \quad 3.70 < U_{10} \leq 11.25, \\ W(U_{10}) &= 4.82 \times 10^{-4}(U_{10} + 1.98)^3; \quad 9.25 < U_{10} \leq 23.09, \end{aligned} \tag{2}$$

where W is percentage total whitecap cover. Note that data have been divided into two overlapping groups according to the measured wind speed, with a regression performed on each group.

[11] In the study of *Goddijn-Murphy et al*. [2011], analysis of the MAP whitecap data set was extended through use of in situ, model, and satellite data for wind and waves. The following $W(U_{10})$ relationship is reported when NASA QuikSCAT satellite wind speed measurements are used:

$$W(U_{10}) = 11.5 \times 10^{-3} U_{10}^{1.86}. \tag{3}$$

2.3. Known Variability of In Situ Whitecap Fraction Observations

[12] The pooling of many historical data sets has demonstrated large scatter in W when plotted solely in terms of

wind speed [*Anguelova and Webster*, 2006]. Part of this variability is likely due to the use of different measurement techniques; this is especially true of earlier data sets where data volume is generally much lower, and measurement techniques less consistent. It has been shown by *Callaghan and White* [2009] that to obtain an individual estimate of W with a fractional error of a few percent, one needs to average over hundreds of individual photographs (or video frames) within an interval short enough to have constant forcing. Analysis of an insufficient number of images—as was the case in many of the earlier studies—can lead to nonconvergent W estimates with larger uncertainties, contributing to data scatter [*Callaghan and White*, 2009].

[13] More recent data sets [*Lafon et al*., 2007; *Sugihara et al*., 2007; *Callaghan et al*., 2008b] show a clustering of W estimates when plotted as a function of U_{10} [*de Leeuw et al*., 2011]. This clustering is indicative of improvements to the extraction of W from photographic data and increases in data volume, although it should be acknowledged that the clustering may in part be due to the similar image processing methodology adopted in these recent studies.

[14] The almost order-of-magnitude scatter that remains is likely an indication that factors other than wind speed play a role in determining whitecap fraction. We discuss these factors below (sections 2.3.2 and 2.3.3), but first we consider how variability in W may in part be a consequence of the sensitivity of W estimates to measurement of different stages of whitecap lifetime.

2.3.1. Active and Residual Whitecaps

[15] Although individual whitecaps are in constant temporal evolution, it is possible to define two distinct phases of a whitecap's life-cycle [*Monahan and Lu*, 1990]. During the active breaking stage, air is entrained into the water column at the wave crest, with associated generation of underwater noise due to bubble formation and fragmentation [*Deane and Stokes*, 2002; *Callaghan et al*., 2013]. As the leading wave crest progresses forward, it continues to entrain air. The resulting surface expression is a dense layer of foam with a visible albedo of around 0.5 [*Whitlock et al*., 1982], termed active (or stage A) whitecaps.

[16] Following active air-entrainment, the whitecap enters its second phase (stage B) as bubbles in the subsurface plume rise to the surface due to buoyancy and turbulent forces. Once at the surface, the lifetime of risen bubbles is dictated by a combination of seawater chemistry (e.g., salinity, saturation levels of dissolved gases), turbulent forces, thin film fluid drainage, and stabilizing or destabilizing forces [*Callaghan*, 2013]. The gradually decaying surface foam layer persists as long as there is a sufficient flux of bubbles to the surface. While subsurface and surface parts of the whitecaps are closely related, the surface foam layers are the subject of interest for microwave remote sensing, excluding deeper bubble plumes [*Anguelova and Gaiser*, 2011].

[17] Whilst many authors have aimed to report measurements of active or residual whitecaps only, the task of separating these signals in photographic data is not straight forward. Furthermore, it is probable that due to the lack of consistency between different measurement techniques used, estimates of W from an individual data set are somewhat conditional on the measurement technique.

[18] *Callaghan et al*. [2012] suggest that much of the scatter between whitecap fraction estimates from different data sets could be due to the variability in foam decay times between different observations. Such variability can significantly affect estimates of residual whitecap fraction, which is known to dominate measurements of total W [*Monahan and Lu*, 1990; *Callaghan et al*., 2012]. It has been shown that factors such as the scale (or intensity) of breaking waves [*Jessup et al*., 1997; *Callaghan et al*., 2012], sea surface temperature [*Bortkovskii and Novak*, 1993], salinity [*Monahan and Zietlow*, 1969; *Peltzer and Griffin*, 1987], and surfactant concentration [*Callaghan et al*., 2012, 2013], can influence the lifetime of foam layers. It is therefore possible that a large degree of variability in W may be attributed to these effects (see section 2.3.3).

[19] The remote sensing signature of foam layers at different frequencies has been related to characteristics of the foam layer, specifically the foam layer thickness [*Anguelova and Gaiser*, 2011]. With satellite estimates of W, it is possible to differentiate between foam of different thicknesses, and thus make some distinction between active and residual whitecaps (section 3.1.2).

2.3.2. Influence of the Wavefield

[20] Over recent years, there has been increased focus on the effect of the wavefield on W. Several recent whitecap data sets include an assessment of how the wavefield may affect W, often through classifying W measurements by a measure of the degree of wave development, and then fitting a $W(U_{10})$ curve for each class.

[21] *Stramska and Petelski* [2003], working with data obtained in the North Atlantic, categorized measurements of W by the corresponding wave conditions; this was achieved by comparing measured significant wave height, H_s, with that expected for a fully developed sea [*Pierson et al*., 1955]. They concluded that at a given wind speed, a developed sea should result in a slightly higher whitecap fraction than that of an undeveloped sea, suggesting that the wind duration or fetch is an important factor in determining W.

[22] *Sugihara et al*. [2007] found evidence that whitecaps are produced most actively under the condition of a pure wind sea, and that W is suppressed by swell. The authors find that in conditions of a pure wind sea, at a given value of U_{10}, W increases with wave age, supporting the conclusions of *Stramska and Petelski* [2003]. In contrast to the above two studies, *Lafon et al*. [2007]—by analyzing photographs taken in a coastal environment—found that there is a peak in W at an intermediate wave age, and that W is likely to be lower both above and below this point.

[23] *Callaghan et al*. [2008b], focusing on a fetch-limited coastal region, observed that: (i) scatter in W was reduced when seas were mixed (i.e., when the spectral intensity of wind waves is of the same order of magnitude as the swell) rather than swell-dominated, (ii) swell-dominated seas result in overall lower values of W than mixed seas (as in *Sugihara et al*. [2007]), and (iii) the presence of a tidal current can augment W estimates under certain conditions.

[24] Most recently, *Goddijn-Murphy et al*. [2011] provided evidence that, at a given wind speed for higher winds ($U_{10} > 10$ m s^{-1}), W is slightly larger in conditions of developed seas (mostly associated with decreasing winds) as opposed to developing seas (increasing winds). *Callaghan et al*. [2008a], using the same data set of W estimates,

had previously come to the same conclusion, reporting higher values of W in cases of decreasing winds (developed seas). *Goddijn-Murphy et al*. [2011] also concluded that whitecap fraction is generally reduced in swell-dominated conditions compared to wind sea conditions in cases of cross swell (angle between direction of wind and swell waves between $\pm 45^\circ$ and $\pm 135^\circ$).

[25] In evaluating the effect of the wavefield on W, it can prove difficult to isolate the effect of the wavefield because of inherent correlations between wind speed and measures of the degree of wave development. Many different measures of sea state have been adopted; these vary in how exactly the degree of wave development should be defined in terms of readily available measurements. Both *Stramska and Petelski* [2003] and *Sugihara et al*. [2007] consider the effect of wave development on W; however, the classification of *Stramska and Petelski* [2003] is based on significant wave height only, which may include contributions from swell, while *Sugihara et al*. [2007] used directional frequency wave spectra to separate swell-dominated from pure wind seas. This makes a direct comparison of their results questionable.

[26] On a practical level, individual in situ data sets are likely to span only a narrow range of possible wave conditions due to the temporal and spatial limitations of an individual field campaign, so that a direct comparison of results between studies may not be viable.

2.3.3. Influence of Other Environmental Factors

[27] It has proven difficult to quantify the dependence of W on sea surface temperature (SST). Only a handful of studies of whitecap fraction consider this effect; furthermore, where data for SST does exist, conditions are often limited to a small range of temperatures.

[28] Both *Monahan and O'Muircheartaigh* [1986] and *Spillane et al*. [1986] found evidence that increasing SST can increase the exponent in a W-U_{10} power-law fit, but with no overall increase in *W. Monahan and O'Muircheartaigh* [1986] reason that the true cause of such a result is the inherent correlation between SST and average duration of high wind events; at higher latitudes (lower SSTs), the average duration of these events is shorter, leading to a wave spectrum that is not fully developed. It is worth noting that these results rely on a comparison of multiple different data sets obtained at different SSTs. Given the different ranges of other conditions encountered by the various studies, the conclusions must be treated with some caution.

[29] *Bortkovskii and Novak* [1993] compiled a much larger data set, including both their own measurements in a range of water temperatures, and those of other research groups. They found that the rate of wave breaking increased with increasing SST, but that the lifetime of the resulting foam patch decreased. The net result on total whitecap fraction is unclear.

[30] Both *Monahan and O'Muircheartaigh* [1986] and *Bortkovskii and Novak* [1993] ascribe the temperature dependence of wave breaking to the associated changes in viscosity. *Monahan and O'Muircheartaigh* [1986] hypothesize that as viscosity decreases (increasing SST) there is less viscous dissipation in waves, and hence more energy available for wave breaking. They also note that with lower water viscosity the bubble size distribution shifts to smaller bubbles [*Pounder*, 1986], which have lower terminal velocities, resulting in increased foam lifetime and thus higher W. *Wu* [1988] and *Stramska and Petelski* [2003] reported no systematic trends in W with SST. In summary, whilst SST can alter W through several different mechanisms, its overall effect on W is not yet clear.

[31] Atmospheric stability is thought to affect W through its influence on the surface momentum flux. The air-sea temperature difference $\Delta T = T_a - T_s$ is often used as a proxy for atmospheric stability—a negative ΔT represents unstable conditions, a positive ΔT stable.

[32] *Monahan and O'Muircheartaigh* [1986] find evidence for greater values of W under unstable conditions than stable conditions at the same wind speed, with W increasing by nearly 10% per °C, at a fixed wind speed. *Wu* [1988] concluded that W will increase as conditions become more unstable, based on an hypothesized relationship between the drag coefficient and ΔT. However, *Stramska and Petelski* [2003] found no evidence of a relation between ΔT and W at a given wind speed.

[33] *Monahan and Woolf* [1988] quantified the stability effect on active and residual whitecap fractions separately. Estimates using their empirical expressions show that the largest changes resulting from stability effects would be on stage A whitecaps with an increase of a factor of 7 from neutral to unstable conditions with $\Delta T = -10^\circ\mathrm{C}$; the increase in stage B whitecap fraction would be a factor of 2.4.

[34] Again, there is no general consensus as to the effects of atmospheric stability on W; those trends that have been observed are small relative to the spread of data.

[35] Whilst the salinity difference between freshwater and saltwater can have a large effect on the persistence of bubble plumes, and thus W [*Monahan and Zietlow*, 1969], the effect is expected to be much more subtle over the relatively small range of salinity variations encountered in the open oceans. *Peltzer and Griffin* [1987] demonstrated that changes to foam lifetime due to salinity are insignificant in the open ocean.

[36] The role surface-active substances (surfactants) play in modulating W in the open ocean has yet to be evaluated, although some laboratory studies do exist [*Garrett*, 1967; *Scott*, 1986; *Peltzer and Griffin*, 1987]. Recently, *Callaghan et al*. [2013] confirmed that the presence of surfactants acts to stabilize surface bubbles and so increase whitecap decay times. As the concentration of surfactants is known to vary markedly over the global oceans [*Falkowski et al*., 1998; *McClain et al*., 2004], it is plausible that presence of such material can significantly affect residual whitecap fraction.

2.4. Need for Global Measurement of Whitecap Fraction

[37] In situ observations, while instrumental in gaining knowledge of W so far, have their limitations. Sampling frequency and data volume are still low, although most recent data sets have benefited from increases to both data volume, through use of automated systems [*Moat et al*., 2009], and improvements in image processing techniques, which increase the average number of images that can be analyzed for an individual estimate of W [*Callaghan and White*, 2009; *Kleiss and Melville*, 2011]. Field

measurements are often limited both spatially and temporally, obtaining measurements in a limited range of conditions. Most in situ data sets have been obtained in near-coastal, fetch limited conditions, and at high latitudes with cold waters [*Anguelova and Webster*, 2006]; data from the open ocean and warm waters (SST $>17^{\circ}$C) are very sparse.

[38] In contrast, satellite-based estimates of W can provide long term, consistent, global estimates of whitecap fraction. Furthermore, with accompanying measurements of many different variables, a thorough study of the variability in whitecap fraction is now viable.

3. Methods

3.1. Satellite-Based Estimates of Whitecap Fraction

3.1.1. Passive Microwave Remote Sensing of Whitecaps

[39] Microwave radiometry is a well-developed passive remote sensing technique that uses the natural emissivity of the ocean surface in its various states—smooth, roughened by small and large scale waves, and covered with sea foam [*Ulaby et al*., 1981, chap. 4]. Changes in ocean surface emissivity are observed by microwave radiometers as changes to the brightness temperature T_B of the ocean surface.

[40] *Anguelova and Webster* [2006] demonstrated the feasibility of estimating W from routine satellite measurements of T_B at 19 GHz, horizontal polarization. This initial algorithm used T_B observations from the Special Sensor Microwave Imager (SSMI/I) [*Wentz*, 1997], a radiometer flown on satellite platforms F8 to F17 of the United States Department of Defense since 1987 and operating at four frequencies between 19 GHz and 85 GHz. The algorithm for estimating W combines satellite T_B observations with models for the rough sea surface and foam-covered areas (whitecaps). An atmospheric model is used to remove the influence of the atmosphere from the satellite measured top-of-atmosphere T_B, in order to obtain the changes in T_B at the ocean surface. Wind speed U_{10}, wind direction U_{dir}, SST at the ocean surface, and atmospheric variables such as water vapor and cloud liquid water are necessary as inputs to the atmospheric, roughness, and foam models. Although various models and many variables are involved in the algorithm estimating W, for simplicity we denote this the $W(T_B)$ algorithm.

[41] The algorithm for estimating W has since been improved in several respects [*Anguelova et al*., 2009]. Notably, more physically robust models for rough and foam-covered surfaces are now employed [*Bettenhausen et al*., 2006; *Johnson*, 2006; *Anguelova and Gaiser*, 2013], as are independent data sources for input variables in the $W(T_B)$ algorithm. Details on the improved $W(T_B)$ algorithm will be given in a future paper; below we briefly summarize information relevant for this study.

[42] The use of independent input data sets in the $W(T_B)$ algorithm has been possible due to newly available T_B observations since 2003—in addition to those of SSM/I—from the microwave radiometric sensor WindSat, onboard the Coriolis satellite [*Gaiser et al*., 2004]. WindSat operates at five frequencies, from 6 GHz to 37 GHz, thus providing more T_B data suitable for remote sensing of whitecaps than SSM/I [*Anguelova and Gaiser*, 2011]. The Coriolis satellite completes 14 orbits per day, with ascending (northbound Equator crossing) and descending (southbound Equator crossing) passes at local times of approximately 18:00 and 06:00, respectively. There are 80 pixels within the WindSat swath with an approximate spacing of 12.5 km across the swath and along the satellite track [*Bettenhausen et al*., 2006]. At the lowest level, each pixel within the WindSat swath represents a T_B (or W) value averaged over an area of 50 km $\times$ 71 km. Each W value resulting from such an intrinsic spatial averaging of satellite instantaneous samples is analogous to the temporal averaging required to produce stable W values from instantaneous photographic data (section 2.3). WindSat T_B data at higher swath resolutions (i.e., pixel value averaged over an area of 35 km $\times$ 53 km or 25 km $\times$ 35 km) are also available, but the work here uses whitecap fraction estimates at the low resolution.

[43] Use of T_B data from WindSat in the $W(T_B)$ algorithm allows independent use of SSM/I data (water vapor and cloud liquid water) for the atmospheric correction. In addition, the input variables U_{10}, U_{dir}, and SST to the atmospheric, roughness, and foam models in the $W(T_B)$ algorithm are also compiled from independent sources (section 3.1.3).

3.1.2. Whitecap Database

[44] Whitecap fraction estimates were obtained by running the $W(T_B)$ algorithm for all five WindSat frequencies and both horizontal and vertical polarizations at swath resolution. All available WindSat orbits for 2006 with both ascending and descending passes were used. A subset of this pool of raw swath data for whitecap fraction was then used to compile a more tractable database of satellite-based W estimates, accompanied by six meteorological and oceanographic variables; hereafter we refer to this database as "W database." The compilation of the W database involved three main activities: (i) devising a criterion to choose a subset of all W data; (ii) gridding the W values from swath resolution into regular global maps; and (iii) matching additional variables to the gridded W values. The following briefly describes activities (i) and (ii); section 3.1.4 informs on (iii).

[45] The W database consists of whitecap fraction values at two frequencies—10 GHz and 37 GHz, horizontal polarization. The choice to work with only these two frequencies, instead of all five frequencies available from WindSat, is based on two considerations. First, the $W(T_B)$ algorithm for satellite-based W estimates is still a work in progress. This W database is an intermediate stage in the $W(T_B)$ algorithm development which can be used to evaluate the utility of the W data, and identify how best to improve the $W(T_B)$ algorithm. Second, recent work on the electromagnetic properties of the sea foam, including the penetration depth of different microwave frequencies through sea foam [*Anguelova and Gaiser*, 2011], shows that each radiometric frequency has a different sensitivity to different stages of the whitecap. While all WindSat frequencies would react to foam thicker than 1 cm, as the frequency decreases from 37 GHz to 6 GHz, its sensitivity to thinner foam decreases. The lower limit of detectable foam thickness for 37 GHz is around 1 mm; for 10 GHz it is 4 mm; and for 6 GHz it is around 1 cm. Because thick foam is associated with the active whitecaps while thin foam characterizes residual

whitecaps [*Anguelova and Gaiser*, 2011], we expect that W estimates at 10 GHz will predominantly be representative of active, stage A (section 2.3.1), whitecaps and to some extent residual foam (stage B) when it is thicker, e.g., at higher wind speeds. At 37 GHz, W estimates will represent total whitecap cover (stages A and B).

[46] The swath W values at 10 GHz and 37 GHz were gridded onto a $0.5^\circ \times 0.5^\circ$ grid. For each grid cell, an average value of all swath W samples falling within the cell is calculated. These cell-averages for each frequency, hereafter referred to as W_{10} and W_{37}, represent a mean estimate of whitecap fraction for the cell at the local time of the satellite overpass. The gridding procedure allows some useful statistics to be obtained for the swath samples contributing to a given grid cell. These include the root-mean-square (rms) error, standard deviation σ_W, and count (the number of individual swath samples averaged to obtain the daily mean W for the cell).

3.1.3. Basic Additional Variables

[47] Whitecap fraction data at swath resolution are matched in time and space with six meteorological and oceanographic variables; wind speed U_{10}, wind direction U_{dir}, SST, air temperature T_a, significant wave height H_s (defined as $4\sqrt{E}$, where E is total wave energy), and peak wave period T_p (defined as the period corresponding to the highest peak in the one-dimensional frequency spectrum of the wavefield). These basic additional variables are taken from independent sources.

[48] Wind vector (U_{10} and U_{dir}) is taken from the SeaWinds microwave scatterometer on-board the QuikSCAT satellite (http://winds.jpl.nasa.gov/missions/quikscat). The matching criterion between WindSat and SeaWinds measurements is within 25 km and 60 min.

[49] When a SeaWinds matchup is not available, U_{10} and U_{dir} from the model output (every 6 h) of the Global Data Assimilation System (GDAS) of National Centers for Environmental Prediction (NCEP) is used. GDAS is the system used by the NCEP global forecast model to place myriad observations (including those of QuikSCAT) into a gridded model space for the purpose of initializing weather forecasts with observed data (http://www.ncdc.noaa.gov/model-data/global-data-assimilation-system-gdas). We use GDAS outputs closest in time and spatially interpolated to the location of the WindSat data.

[50] To ensure that use of two different wind speed sources does not introduce bias, we explore the distribution of swath resolution U_{10} values from QuikSCAT and GDAS, for 1 October 2006 (Figure 1a). The shapes of the probability density functions for the two sources are similar.

[51] Differences of a few percent are visible at low wind speeds ($U_{10} < 5$ m s^{-1}) where QuikSCAT values are higher than those of GDAS; GDAS values are higher for $U_{10} > 11$ m s^{-1}. Note that this is not a comparison of paired QuikSCAT—GDAS values for U_{10} at a given location; at each point we have either a QuikSCAT or GDAS value. For the U_{10} values considered in Figure 1a, we find that in general GDAS has more counts at high latitudes and low latitudes, while in the midlatitudes, a larger count is from QuikSCAT values. It is therefore logical that GDAS gives higher probability for high winds than QuikSCAT, while QuikSCAT gives higher probability for low winds. Figure 1b shows a histogram of gridded wind speed values coupled with W data for 2006.

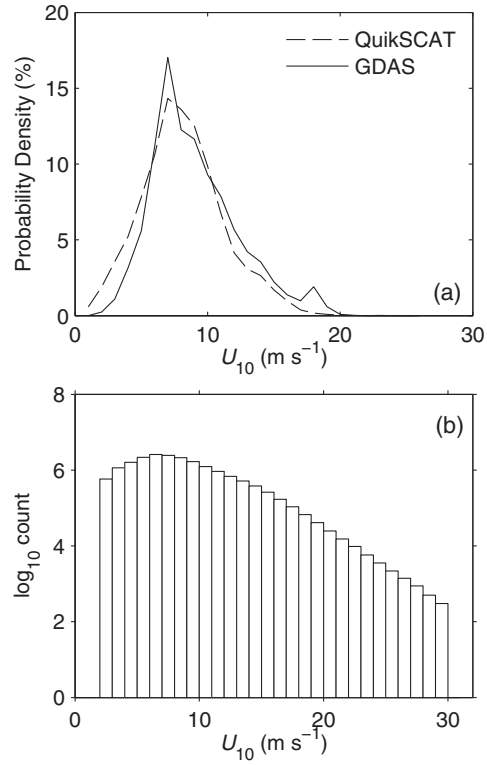

Figure 1. (a) Probability density function of swath resolution U_{10} values from QuikSCAT and GDAS for 1 October 2006. (b) The number of individual gridded W estimates obtained for each 1 m s^{-1} wind speed bin over the course of 2006.

[52] Data for SST and T_a (at 2 m above the surface) are also from GDAS. H_s and T_p values are from NCEP Wave Watch III (WW3) model. We have used the historical archive of wave hindcast results produced with version 2.22 of WW3 at 3 h intervals (http://polar.ncep.noaa.gov/waves/implementations.shtml). The input variables for WW3 are from GDAS. The WW3 model also gives peak wave direction, but it is not currently included in the database. The temporal and spatial matching criteria for WindSat and WW3 data are as those for GDAS. Table 1 summarizes information for these variables, including their spatial resolutions, use, and access.

[53] All these variables, matched up initially to WindSat data in swath resolution, are gridded in the same way as the W estimates (section 3.1.2). Mean daily values, as well as statistics (root-mean-square error, standard deviation, and count), are obtained for each variable for each grid cell.

3.1.4. Data Used in This Study

[54] This study makes use of the gridded satellite-based estimates of whitecap fraction from both 10 GHz and 37 GHz, W_{10} and W_{37}. Data for all of 2006 are used in daily and monthly format. Figures 2a and 2b present daily global maps of W_{10} and W_{37} along both ascending and descending passes for 1 October 2006. The resulting spatial match is patchy because the ascending and descending passes of the Coriolis and QuikSCAT satellites are out of phase. Figures 2c and 2d show monthly maps for October 2006.

Table 1. Sources of Database Variables, With Resolution and Data Access

Model/Sensor (Satellite) Access	Variable (units)	Grid Resolution	Variable Use
Windsat (Coriolis) Naval Research Laboratory	Brightness temperature T_B (K)	$0.5^o \times 0.5^o$	$W(T_B)$ algorithm
SSM/I (F13) Remote Sensing Systems[a]	Water vapor Cloud liquid water	$0.25^o \times 0.25^o$	$W(T_B)$ algorithm
SeaWinds (QuikSCAT) PODAAC/JPL[b]	Wind speed U_{10} (m s^{-1}) [c] Wind direction U_{dir} (^{o})	$0.25^o \times 0.25^o$	$W(T_B)$ algorithm & W database
GDAS/NCEP[d] CISL RDA[e]	U_{10}, U_{dir}, SST (^{o}C) Air temperature T_a (^{o}C)	$1^o \times 1^o$	$W(T_B)$ algorithm & W database W database
WaveWatch III/ NOAA NCEP[f]	Significant wave height H_s (m) Peak wave period T_p (s)	$1^o \times 1.25^o$	W database
World Ocean Atlas 2005 NOAA[g]	Salinity—surface field	$1^o \times 1^o$	Expand W database

[a]www.remss.com.
[b]Physical Oceanography Distributed Active Archive Center at the NASA Jet Propulsion Laboratory (http://podaac.jpl.nasa.gov).
[c]Satellite wind estimates (such as those from QuikSCAT) are calibrated to equivalent neutral wind speeds [*Kara et al.*, 2008]. Model winds are also corrected to neutral winds.
[d]Global Data Assimilation System, National Centers for Environmental Prediction (http://www.emc.ncep.noaa.gov/gmb/gdas/).
[e]Research Data Archive at Computational and Information Systems Laboratory (http://rda.ucar.edu/datasets/ds083.2/).
[f]National Centers for Environmental Prediction (http://polar.ncep.noaa.gov/).
[g]National Oceanographic Data Center (http://www.nodc.noaa.gov/OC5/WOA05/woa05data.html).

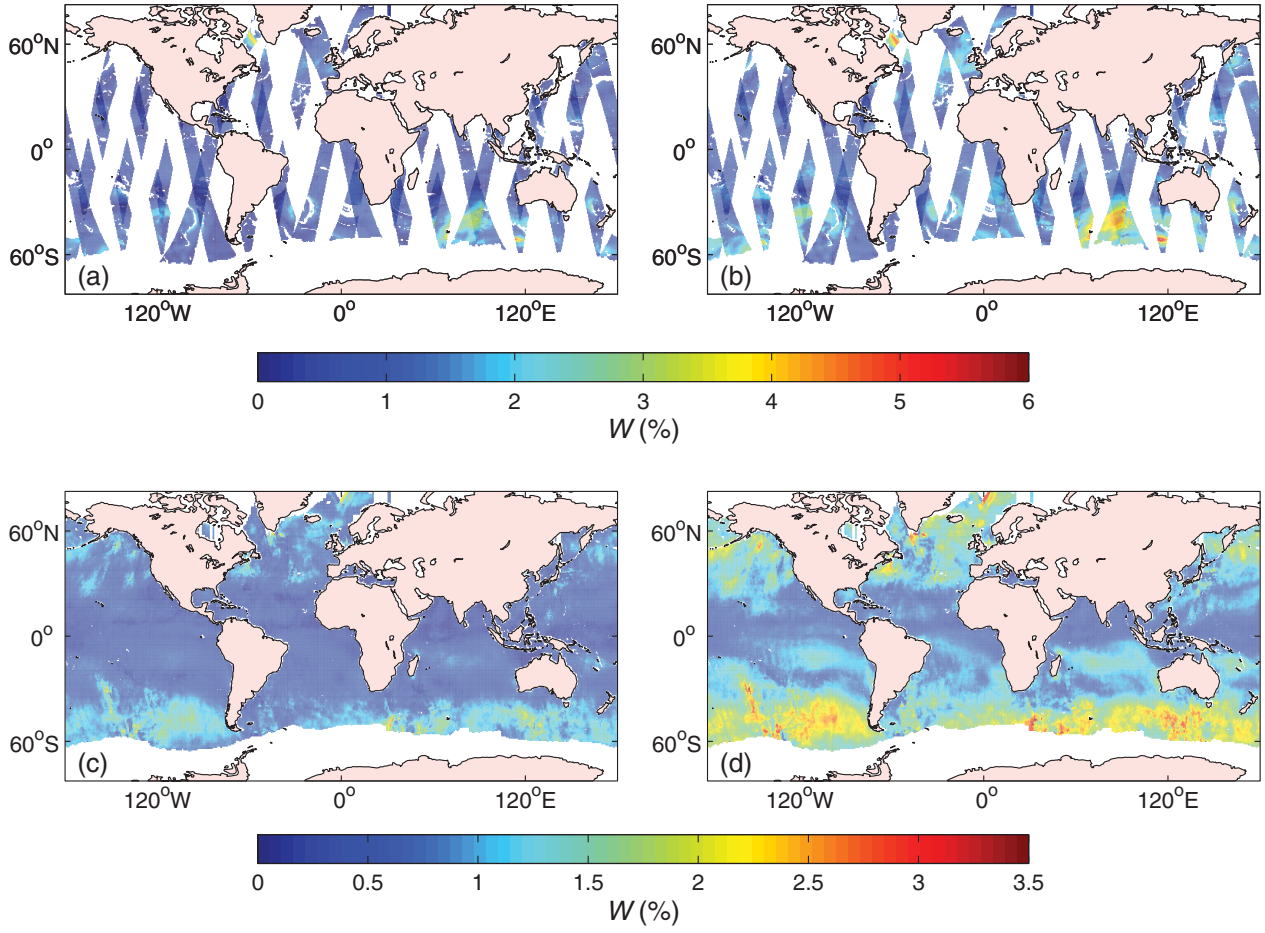

Figure 2. Whitecap fraction (%) as a daily map for 1 October 2006, (a) at 10 GHz, (b) 37 GHz, and as a monthly composite for October 2006, (c) at 10 GHz, and (d) at 37 GHz.

[55] Explicit calculation of the error on individual W estimates is not currently available due to the complex multivariable nature of the $W(T_B)$ algorithm. However, where applicable, we have used the statistics obtained during the gridding process to screen for unreliable W estimates resulting from, for example, a low count in a particular grid cell, or an exceptionally large variation between individual swath samples.

[56] We expect some correlation between W_{10} and W_{37} values and the basic additional variables. The reason is that the same U_{10}, U_{dir}, and SST values used in the $W(T_B)$ algorithm at swath resolution (section 3.1.1) are also entries in the W database in gridded format. We tolerate some correlation because we did not see substantial gains in seeking different sources for U_{10}, U_{dir}, and SST data. For instance, we aim to use all available W estimates, of which there are more than 18 million; this would not have been possible with a more selective temporal and spatial match-up with direct measurements from other satellites or buoys. Gains in using independent data would have also been limited if we used model outputs different from those provided by GDAS (e.g., use of the European Centre for Medium-Range Weather Forecasts (ECMWF)) considering that assimilation of buoy and satellite measurements in any model is a common practice. Indeed, assimilation of the QuikSCAT data in ECMWF and NCEP have led to wind component values differing by at most 1.5 m s^{-1} [*Chelton and Freilich*, 2005].

[57] We expanded our set of six basic variables in the current whitecap database with salinity S. We use monthly mean salinity fields from the NOAA World Ocean Atlas 2005 (WOA05) (accessible online at www.nodc.noaa.gov/OC5/WOA05/pr_woa05.html).

[58] The expansion of the W database with further basic additional variables (e.g., wave direction from WW3, currents, ocean color as a proxy of surfactants) and fully independent data (e.g., wind and SST) is planned future work.

3.2. Derived Additional Forcing Variables

[59] In addition to the variables listed in Table 1 as entries in the W database, several further parameters are constructed to assess their influence on W. Atmospheric surface layer stability is indicated by the air-sea temperature difference $\Delta T = T_a - T_s$. The kinematic viscosity of water, ν_w, is calculated using a combination of daily SST fields and monthly mean salinity fields.

[60] Two dimensionless wind-wave variables are considered. The breaking-wave Reynolds number, defined as:

$$R_B = \frac{u_*^2}{\omega_p \nu_a}, \tag{4}$$

where ω_p is the spectral peak angular frequency of wind waves, and ν_a is the kinematic viscosity of air. The consideration of such a nondimensional variable as an appropriate parameter to describe wave breaking dates back to the work of *Toba and Chaen* [1973], with R_B in its above form first suggested as a parameter to describe whitecap fraction by *Toba and Koga* [1986]. The roughness Reynolds number,

$$R_{Hw} = \frac{u_* H_s}{\nu_w}, \tag{5}$$

is a slightly modified version of that of *Zhao and Toba* [2001], the only difference being the use of the kinematic viscosity of water ν_w instead of ν_a, following the suggestion of *Woolf* [2005].

3.2.1. Measures of Wave Development

[61] Recent in situ studies have strived to explicitly evaluate the role of the wavefield on variability in W. Wave age Φ—defined as c_p/u_*, where c_p is the wave phase velocity and u_* the air-side friction velocity—can be used to infer the stage of development of the sea. Φ can be expressed in terms of readily available measurements as:

$$\Phi = \frac{gT_p}{2\pi\sqrt{c_d}U_{10}}, \tag{6}$$

by using $c_p = gT_p/(2\pi)$ [*Hanley et al.*, 2010]. Here c_d is the drag coefficient, calculated following *Large and Pond* [1981].

[62] We also calculate the mean wave slope *MWS* (also referred to as significant steepness or simply wave slope),

$$MWS = \frac{2\pi H_s}{gT_p^2}, \tag{7}$$

which is a measure of the steepness of the dominant waves. Note the use of the peak wave period in this formulation (the only available wave period measure), as opposed to the mean wave period. Although it has been shown that *MWS* alone cannot predict whether an individual wave will break [*Holthuijsen*, 2007], here we consider this quantity as a bulk measure of the degree of wave development that combines the effects of H_s and T_p. As *MWS* is not explicitly dependent upon wind speed, it is included in our analysis of variability in W once the wind speed dependence has been accounted for (section 4.2.1). The dependence of W on *MWS* has not previously been considered.

3.2.2. Classification of the Wavefield

[63] A different approach to assessing the influence of the wavefield involves categorizing W estimates by degree of wave development. Ideally, spectral wave data would be used to reveal the presence (and relative intensity) of different regimes such as wind sea and swell [e.g., *Sugihara et al.*, 2007; *Callaghan et al.*, 2012]. Detailed wave spectra are not available here; however, it is possible to use the two wave measures available in the current database (H_s and T_p), together with U_{10}, to attempt a broad classification of W estimates by the stage of wave development. A similar approach was adopted in the study of *Stramska and Petelski* [2003], where U_{10} and H_s measurements were used to classify data into three groups; those obtained in undeveloped seas, those obtained in developed seas, and those obtained under conditions of decreasing winds. They note that while this criterion is not exact, it does allow an insight into the effects that sea state can have on W.

[64] Classification by significant wave height is as follows. At each individual grid cell, the recorded value of H_s is compared with H_{fd}, the significant wave height that would be expected given a fully developed sea in

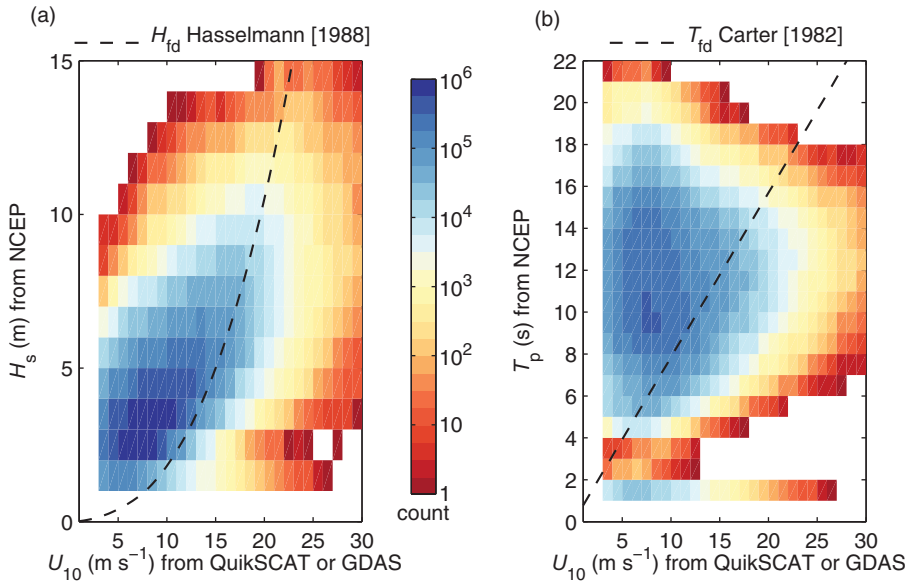

Figure 3. (a) Density plot of U_{10} and H_s for all W estimates from 2006. Also shown is the *Hasselmann et al*. [1988] theoretical relationship relating the two for a fully developed sea (black dashed line). (b) As Figure 3a, but for U_{10} and T_p estimates, and with the *Carter* [1982] relationship overlaid.

equilibrium with the wind. H_{fd} is calculated from the wind-wave relation in the WAM model [*Hasselmann et al*., 1988],

$$\begin{aligned} H_{fd} &= 1.614\times10^{-2}U_{10}^2; \quad 0 < U_{10} \le 7.5, \\ H_{fd} &= 10^{-2}U_{10}^2 + 8.134\times10^{-4}U_{10}^3; \quad 7.5 < U_{10} \le 50. \end{aligned} \tag{8}$$

This relationship defines the sea state as either *swell* when $H_s > H_{fd}$ or *wind sea* when $H_s < H_{fd}$. At the threshold level, where $H_s = H_{fd}$, it is assumed that the seas have just become fully developed.

[65] Similarly, T_p can be used to partition W estimates. A relation predicting the peak wave period of a fully developed sea is given by *Carter* [1982] as:

$$T_{fd} = 0.785U_{10}. \tag{9}$$

[66] The frequency of occurrence of U_{10} and H_s is shown in Figure 3a. It is evident that the vast majority of data points lie above the threshold for a fully developed sea, indicating that a large portion of W estimates have been obtained in swell-dominated seas. The same conclusion can be drawn from Figure 3b, where T_p estimates are used to separate wind sea from swell cases using equation (9).

[67] The results here echo those in the study of *Chen et al*. [2002], who note that there is a systematic swell dominance in the world's oceans, with swell occurring more than 80% of the time in most of the world's oceans. As such, this whitecap data set comprises mostly W estimates obtained under swell affected/dominated conditions. This is in contrast to the many in situ data sets obtained in coastal or fetch-limited regimes, where wind sea conditions are generally more prevalent. This is an important point, and should be noted when comparing findings from this study and those from previous in situ studies regarding the influence of the wavefield on W (section 4.2.1).

[68] With slight modification of the above relationships, we form our own classification system through which the influence of wave development on W is assessed (section 4.2.2). The modification expands the threshold levels defined by (8) and (9) from exact equalities to a narrow range of values representative of fully developed state. According to this system, W estimates are classified as fully developed sea if $(H_{fd}-0.5) < H_s \le (H_{fd}+0.5)$, and $(T_{fd}-1) < T_p \le (T_{fd}+1)$. Estimates are classified as wind sea cases if $H_s \le H_{fd}-0.5$ and $T_p \le T_{fd}-1$. Finally, W estimates are classed as swell if $H_s > H_{fd}+0.5$ and $T_p > T_{fd}+1$.

[69] Following *Sugihara et al*. [2007], we further partition the wind sea cases by the degree of wave development using wave age. Wave ages for wind sea cases have a range $5 \le \Phi \le 31$, with an almost symmetric distribution around the peak frequency of occurrence at $\Phi = 22$. We divide the data classified as wind sea into three groups: $5 \le \Phi < 20$, $20 \le \Phi < 25$, and $25 \le \Phi \le 31$, so that the number of data points in each group is approximately equal.

3.3. Analyses

[70] We examine the dependence of W_{10} and W_{37} on six basic variables (U_{10}, T_a, SST, H_s, T_p and S) and six derived forcing variables (ΔT, v_w, R_B, R_{Hw}, Φ, and MWS). We have performed three main analyses. First, we quantify the dependence of satellite-based W on wind speed alone, then the variability of whitecap fraction due to other factors, and finally we evaluate the relative contribution of each forcing factor to the W variability.

3.3.1. Quantifying the Effects of Wind Speed

[71] To explore the wind speed dependence of satellite-derived W, all estimates in the range $0 < U_{10} \le 30$ m s^{-1} are averaged into wind speed bins of 1 m s^{-1} width (Figure 1b). To investigate how well wind speed alone accounts for the variability in satellite-derived estimates of whitecap fraction, we consider the strength and spatial characteristics

of the correlation between whitecap fraction and wind speed. We calculate a cell-by-cell Pearson product-moment correlation coefficient R from a series of W and wind speed pairs. The number of individual W estimates used to calculate R for a grid cell ranges from 3 to 317, with an average of 140.

[72] Wind direction is one of the basic variables in the W database (Table 1), but we have not analyzed W as a function of U_{dir} because $W(U_{\mathrm{dir}})$ relationship is not pertinent when parameterizing air-sea interaction processes in terms of W. Brightness temperature used to obtain radiometric estimates of W varies with both wind speed and wind direction. This directional dependence comes from the nonuniform distribution of the foam and short (capillary) waves over the profile of the underlying large-scale waves, e.g., the face of a breaking wave has higher emissivity than its back [*Wentz*, 1992].

[73] Wind direction could, however, be useful as a means of determining the fetch of the wind so that the history of the wavefield can be inferred [*Callaghan et al*., 2008a]. It has been shown that whitecap fraction is dependent upon whether the wind is aligned with or against the waves and/or currents [*Sugihara et al*., 2007; *Callaghan et al*., 2008a]. To investigate such variability, one requires detailed spectral information, such as directional wave spectra [*Sugihara et al*., 2007], usually provided by models at specific regions but not on a global scale. At this stage of development, the W database does not contain information necessary for systematic study of directional W variability. Work on this topic, however, should be pursued as the W algorithm is further improved.

3.3.2. Quantifying the Effects of Secondary Factors

[74] To investigate sources of variability in W, we first remove the strong wind speed dependence. Prior to this procedure we omit all W estimates that have a relative standard deviation (σ_W/W) above 0.2—approximately 10% of estimates. W estimates failing this condition mostly occur in low winds, close to the threshold value for whitecap formation ($\sim$4 m s^{-1}). We choose to work with all remaining W estimates for which 4 m s$^{-1} \leq U_{10} \leq 20$ m s^{-1}, thus excluding both low and very high wind speed regimes, where data are much sparser and removal of a mean wind speed trend would be dubious.

[75] The removal of the wind speed trend is as follows. All accepted estimates from 2006 are first binned by wind speed. Here we use wind speed bins of width 0.5 m s^{-1} to reduce the sensitivity of W to changes in U_{10} over the range of an individual wind speed bin. A mean whitecap fraction $\overline{W}$ is calculated for each wind speed bin. Then, all W estimates in each of the 32 wind speed bins are further binned by the variable under investigation, and a mean whitecap fraction $\overline{\overline{W}}$ is obtained for each subbin. Normalizing each subbin mean by $\overline{W}$ results in the ratio $\overline{\overline{W}}/\overline{W}$, essentially showing the deviation from the mean wind speed behavior over the range of each secondary forcing variable.

[76] The decision to represent our results in terms of normalized whitecap fraction (rather than as an anomaly) is made through two considerations. We know that W depends strongly on wind speed and expect that the effects of the secondary forcing parameters would be to either enhance or suppress the wind speed effect. The ratio above can represent well such enhancement or suppression of the wind speed influence by the secondary factors. When $\overline{\overline{W}}/\overline{W} > 1$, we can surmise that the considered secondary factor enhances whitecap fraction at the wind speed for which $\overline{W}$ is obtained. When $\overline{\overline{W}}/\overline{W} < 1$, the secondary factor suppresses W at a given $\overline{W}$.

[77] A second consideration is that at this intermediate stage of the whitecap database (section 3.1.2), use of relative, rather than absolute, values is more pertinent. As the $W(T_B)$ algorithm continues to develop and improve, the absolute values may change. Meanwhile, the trends seem to be robust considering that the observation of more uniform latitudinal distribution of W documented with the initial implementation [*Anguelova and Webster*, 2006] remains for satellite-based estimates W_{37}, that account for total (active plus residual) whitecap fraction.

3.3.3. Principal Component Analysis

[78] To explore how successful each variable is in describing variability in W, and thus rank their importance, we use Principal Component Analysis (PCA) on all database estimates following *Anguelova et al*. [2010]. PCA is first performed on data sets comprising W and each of the 12 variables. To ensure that the dominant U_{10} signal does not mask the variance explained by additional factors, PCA is also performed on data sets comprising W, U_{10}, and each secondary variable (11 data sets). To perform PCA, it is first required that all data are standardized—a transformation is applied so that each data set has a mean of zero and a variance of one [*Preisendorfer and Mobley*, 1988].

4. Results

4.1. Wind Speed Dependence

[79] In Figure 4a, we compare satellite-based W, at 10 GHz and 37 GHz, to three $W(U_{10})$ parameterizations; that of *Monahan and O'Muircheartaigh* [1980] (MM80), *Callaghan et al*. [2008a] (Cal08), and *Goddijn-Murphy et al*. [2011] (GM11). It is apparent that both W_{10} and W_{37} have a weaker wind speed dependence than the MM80 and Cal08 formulations based on in situ U_{10} values, indicative of overestimation of satellite retrieved W at low wind speeds, and underestimation at higher wind speeds. However, W_{10} is close to the GM11 formulation, which uses the same set of W estimates as *Callaghan et al*. [2008a], but satellite (rather than in situ) U_{10} data. At $U_{10} > 20$ m s^{-1}, W_{37} begins to level off, causing W_{37} to fall lower than W_{10}. This behavior looks somewhat suspicious considering our interpretation of the two different estimates and perhaps points to an issue with the retrieval—one that should be explored in future work if this feature persists.

[80] At moderate wind speeds (7 m s$^{-1} < U_{10} < 12$ m s^{-1}), the satellite retrievals compare reasonably well with the Cal08 parameterization (Figure 4b). At the global average oceanic wind speed of $U_{10} = 7$ m s^{-1}, W_{10} differs by just 0.2% from Cal08, while W_{37} differs by 0.8%.

[81] Figure 4c highlights good agreement between the satellite W estimates and those from the GM11 parameterization. Absolute differences between W_{10} and GM11 are small for wind speeds lower than 12 m s^{-1}; above this the difference grows, reaching 0.9% at $U_{10} = 24$ m s^{-1}. The difference between W_{37} and GM11 increases with wind speed to a maximum of 1.5% at $U_{10} = 20$ m s^{-1}. We must be cautious with regards to the comparison between

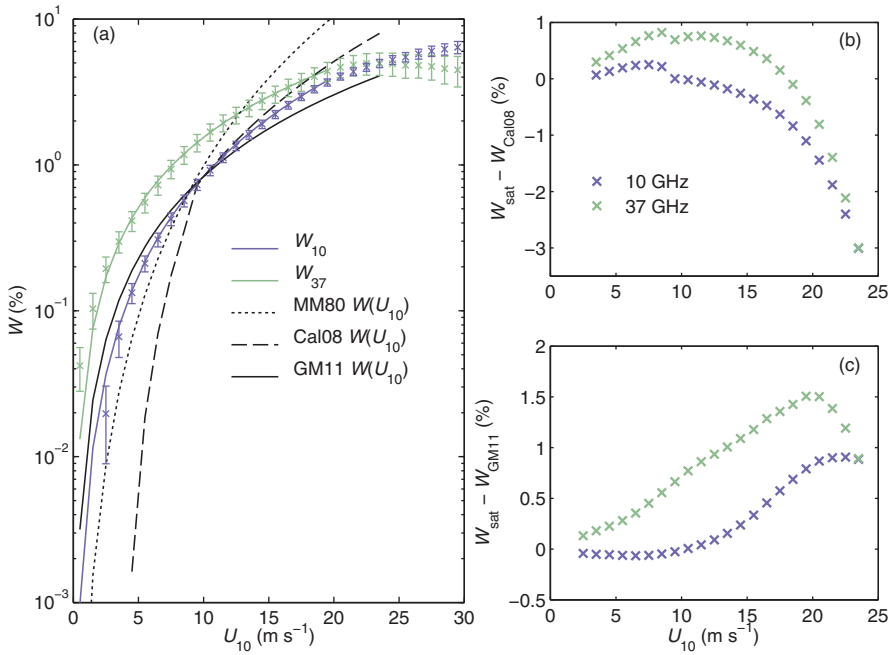

Figure 4. (a) Wind speed dependence of satellite-derived W (W_{10} and W_{37}), two $W(U_{10})$ parameterizations from in situ data—that of *Monahan and O'Muircheartaigh* [1980] (MM80) and *Callaghan et al.* [2008a] (Cal08)—and a $W(U_{10})$ parameterization using satellite winds [*Goddijn-Murphy et al.*, 2011] (GM11). Error bars indicate the standard deviation. (b) The absolute difference between W_{10} and W_{37} and the Cal08 relationship. (c) As Figure 4b but the comparison is made with the GM11 parameterization.

satellite and in situ W estimates at high wind speeds ($U_{10} > 20$ m s^{-1}) because of the sparseness of in situ estimates, extrapolation of some of the functions beyond the range of their source data, and the uncertain validity of the retrieval algorithm at high winds.

[82] There is no signal for W_{10} below 2 m s^{-1}, whereas for W_{37} there is a small signal for 0 m s$^{-1} \leq U_{10} < 2$ m s^{-1}, the result of a handful of instances where foam has been detected. These winds speeds are below the suggested threshold for visible air-entraining breaking waves of ~4 m s^{-1} [*Callaghan et al.*, 2008a]. Whilst there is likely to be little (or no) whitecap formation at these wind speeds, microwave radiometers may detect small amounts of residual long-lived foam from infrequent small wave breaking events, which may be missed in photographic analysis.

[83] W_{10} and W_{37} are parameterized as functions of wind speed by fitting power laws to the bin means. We fit both W_{10} and W_{37} over the same wind speed range, thus excluding W_{37} estimates for the first two bins, where W_{10} estimates are always zero. The functions are valid up to a maximum wind speed of 20 m s^{-1}:

$$\begin{aligned} W_{10} &= 4.6\times10^{-3}\times U_{10}^{2.26}; \quad 2 < U_{10} \leq 20 \text{ m s}^{-1}, \\ W_{37} &= 3.97\times10^{-2}\times U_{10}^{1.59}; \quad 2 < U_{10} \leq 20 \text{ m s}^{-1}, \end{aligned} \tag{10}$$

where W is expressed in %.

[84] The W_{10} is closest to the other functions shown, particularly GM11, while W_{37} is substantially higher over most of the wind speed range.

[85] The correlation coefficients of W_{10} and W_{37} at each grid point are shown in Figure 5; for W_{10} over 95% of points have a correlation > 0.95, while for W_{37} this fraction is 89%. The small number of cells below these thresholds is generally either close to land, or has a low count rate over the year. Correlation with wind speed is higher for W_{10}, suggesting that more variability in W_{37} can be attributed to factors other than U_{10}. Furthermore, because R is a measure of the strength of a linear relationship, the correlations reported here may be biased low, more so in the case of W_{10} which has a more nonlinear dependence on wind speed.

[86] The spatial structure of variations in correlation coefficient differs between W_{10} and W_{37}. Correlation between U_{10} and W_{10} is highest in low-latitude regions. Slightly lower values of R are found in the midlatitudes, where the variability in wind speed (and wavefield) is higher. Correlation is more variable for W_{37}, with areas of lower correlation found in both low average wind speed regions (equatorial Pacific) and regions where wind speed is on average much higher, but highly variable (Southern Ocean). We note that the spatial patterns in R are not explained by differences in the U_{10} range which has potential to distort the statistic.

4.2. Dependence on Secondary Factors

[87] In the following analysis of the influence of secondary factors (Figures 6, 7, 9, and 10), the panels for normalized W_{10} and W_{37} have the same y scales for easy comparison. We consider two main features in all the figures. One is the overall trend of normalized whitecap fraction $\overline{\overline{W}}/\overline{W}$ over the full range of possible values of each secondary factor and its deviation above and below unity. Another is the spread within a family of curves, color coded to show these deviations by wind speed bin.

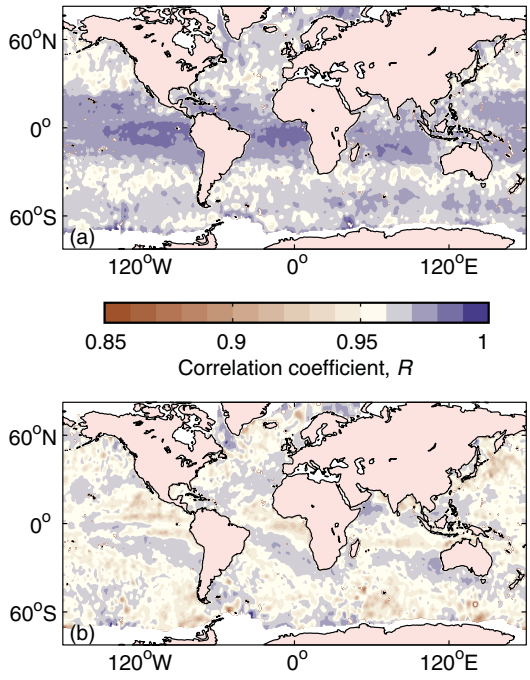

Figure 5. Global maps of cell-by-cell Pearson's correlation coefficient R for U_{10} and (a) W_{10}, and (b) W_{37}. Sources for W and U_{10} are listed in Table 1. Data comprise all estimates from 2006.

4.2.1. Dependence of Whitecap Fraction on Wave Variables

[88] The variability of whitecap fraction as a function of wave parameters is assessed by plotting $\overline{\overline{W}}/\overline{W}$ as a function of H_s, T_p, and MWS (Figure 6). It is evident that the influence of secondary factors on W_{10} (Figures 6a, 6c, and 6e) is much weaker than that on W_{37} (Figures 6b, 6d, and 6f), in regards to both the magnitude of the trends observed and the spread in these trends with wind speed. Additionally, secondary influences are generally stronger with increasing U_{10}.

[89] There is a small (~6%), approximately linear, increase in $\overline{\overline{W}}_{10}/\overline{W}_{10}$ over the range of H_s (Figure 6a). $\overline{\overline{W}}_{37}/\overline{W}_{37}$ increases much more with H_s, particularly in the range $2\,\mathrm{m} < H_s < 6\,\mathrm{m}$ (Figure 6b). In the range $3\,\mathrm{m} < H_s < 5$ m (depending on the wind speed), there is a leveling off, or even reduction in $\overline{\overline{W}}_{37}/\overline{W}_{37}$ at low and moderate wind speeds, while at the highest wind speeds, $\overline{\overline{W}}_{37}/\overline{W}_{37}$ continues to increase, but at a much slower rate. The change in $\overline{\overline{W}}_{37}/\overline{W}_{37}$ increases from 15% to 20% over the range of H_s with increasing wind speed.

[90] As for H_s, the influence of T_p is small for W_{10} (Figure 6c) but larger for W_{37} (Figure 6d). For normalized W_{10} there is little variation with T_p at low wind speeds, whereas at the highest wind speeds $\overline{\overline{W}}_{10}/\overline{W}_{10}$ shows a slight (5%) increase with T_p. Likewise, deviations from the mean for $\overline{\overline{W}}_{37}/\overline{W}_{37}$ over the T_p range are much more pronounced for high wind speeds; $\overline{\overline{W}}_{37}/\overline{W}_{37}$ can increase by as much as 20% as we move from a wave period of 5 s to 10 s. At lower wind speeds ($U_{10} < 12$ m s^{-1}), $\overline{\overline{W}}_{37}/\overline{W}_{37}$ peaks at $T_p = 11$ s. For $T_p = 13$ s, changes to normalized W are minimal.

[91] Mean wave slope combines information for H_s and T_p, and so reflects joint changes in both variables. This variable serves as an indicator of the degree of wave development with MWS reducing as waves develop ($MWS > 0.03$), reach wind-wave equilibrium ($MWS \sim 0.03$), and finally become overdeveloped ($MWS < 0.03$) [*Bourassa et al.*, 2001]. Again, variations in normalized W_{10} are small (Figure 6e). There is a clear peak in normalized W_{37} (Figure 6f) for a given wind speed, with the peak values occurring in the range $0.025 < MWS < 0.035$. At the lowest wind speeds, $\overline{\overline{W}}_{37}/\overline{W}_{37}$ begins to rise again at $MWS > 0.045$. The peak in normalized W at or close to the threshold marking wind-wave equilibrium indicates that sea states in equilibrium with the wind result in the largest values of W at a given wind speed.

4.2.2. Degree of Wave Development

[92] The results in the previous section provide a coarse assessment of changes to W due to the wavefield, characterized by three different variables. We examine the dependence of W on H_s, T_p, and MWS again in Figure 7, but with further classification of the data as either wind sea (yellow/red curves) or swell (blue curves). There are a small number of cases where data cannot be classified as either swell or wind sea due to data being categorized as swell based on H_s and wind sea based on T_p, or vice versa. These cases (approximately 10%) are omitted from the analysis.

[93] The trends in normalized W_{10} due to change in H_s are quite similar for wind sea and swell-dominated cases. For normalized W_{37} (panel b), there is some evidence to suggest that the leveling off of normalized W with higher H_s is mostly confined to swell cases, whereas for wind sea conditions, normalized W continues to increase although at a decreasing rate with increasing H_s.

[94] Trends with T_p are somewhat harder to evaluate due to the grouping of wind sea data at low T_p, and swell at high T_p. The influence of T_p on W_{10} at a given wind speed is minimal in swell conditions. A trend of increasing $\overline{\overline{W}}_{10}/\overline{W}_{10}$ is seen for wind sea, whereas for swell there is little change. For W_{37}, the largest deviations from the mean wind speed behavior can be seen for wind seas at $T_p < 8$ s, where seas are likely to be under-developed. Suppression of W_{37} is strongest in this regime at the highest wind speeds; under these conditions, seas will be significantly under-developed.

[95] The results for MWS show that W_{10} is suppressed slightly for wind sea and swell cases either side of $MWS = 0.03$, but with no clear separation between the behavior of the two cases. In conditions where $MWS > 0.03$, nearly all W estimates are classified as wind sea. Here normalized W_{37} increases with MWS at low winds, whereas at higher wind speeds there is a strong decrease with increasing MWS. The latter results in a large suppression of W_{37}; in such conditions, the magnitude of the wind in excess of equilibrium is at its largest [*Bourassa et al.*, 2001]. We expect cases for which $MWS < 0.03$ to correspond to well-developed seas; however, W estimates can still be classified as wind sea based on the classification using H_s and T_p values. In this MWS regime, there is a decrease in normalized W_{37} with decreasing MWS for both swell and wind sea cases, although this decrease is more rapid in wind seas.

[96] We further assess the influence of the wavefield in Figure 8 by classifying data as either swell, fully developed, or wind seas, with wind seas further classified by

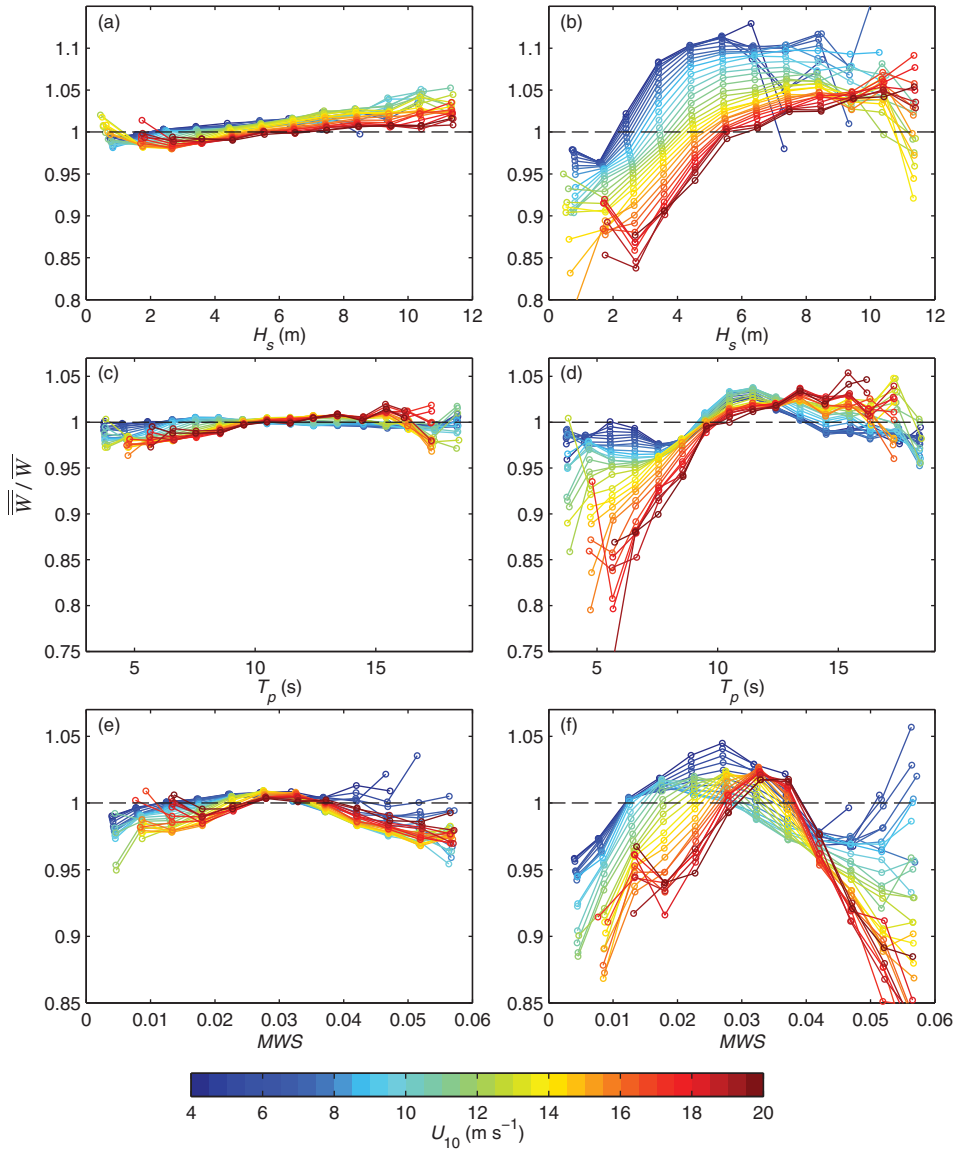

Figure 6. The dependence of (a, c, and e) $\overline{\overline{W}}_{10}/\overline{W}_{10}$ and (b, d, and f) $\overline{\overline{W}}_{37}/\overline{W}_{37}$ on (top) significant wave height, (middle) peak wave period, and (bottom) mean wave slope.

wave age (section 3.2.2). Using 1 m s^{-1} bins to increase the number of W estimates in individual bins, we calculate wind speed bin-averaged means, $\overline{W}$, for each of the classes. The ratios $\overline{W}/\overline{W}_{\mathrm{fd}}$ are calculated for swell and three wave age ranges of wind sea to quantify enhancement or suppression of W, at a given wind speed, due to under-developed (wind sea) or overdeveloped (swell) wave states. These are shown in Figure 8a for W_{10}, and Figure 8b for W_{37}.

[97] For W_{10}, deviations from W_{fd} in swell and wind seas are almost negligible for 9 m s$^{-1} < U_{10} < 20$ m s^{-1}. For 3 m s$^{-1} < U_{10} < 7$ m s^{-1}, there is enhancement of W_{10} for wind seas compared to fully developed sea states. However, this trend could be a result of the limitations of such a classification for low wind speeds; W estimates for $U_{10} < 7$ m s^{-1} are almost always classified as swell-dominated, with only 1–2% classified as fully developed. Therefore, calculation of $\overline{W}_{\mathrm{fd}}$ at these wind speeds may suffer from poor statistics.

[98] For W_{37} (Figure 8b), deviations from W_{fd} are generally larger. Over much of the wind speed range, W is enhanced in swell-dominated conditions, and suppressed in wind seas. Interestingly, for 7 m s$^{-1} < U_{10} < 13$ m s^{-1}, the largest suppression of W_{37} occurs in wind seas with highest wave ages ($25 \leq \Phi \leq 31$). At higher wind speeds ($U_{10} > 14$ m s^{-1}), W_{37} is suppressed most in the youngest wind seas ($5 \leq \Phi < 20$), with $\overline{W}$ ~10% lower than $\overline{W}_{\mathrm{fd}}$.

4.2.3. Dependence on Other Environmental Factors

[99] The dependence of W upon SST and the viscosity of water are examined in Figure 9. The viscosity of water, although strongly related to SST, is a more fundamental quantity which takes into account the effect of salinity.

[100] The influence of SST on W_{10} is very small, with a slight reduction in $\overline{\overline{W}}_{10}/\overline{W}_{10}$ at the highest values of SST and for the highest wind speeds only (Figure 9a). Normalized W_{37} is near constant for SST < 20°C, but drops off rapidly for SST > 20°C (Figure 9b). Whitecap fraction is enhanced at a given wind speed by up to 12% at low temperatures. These deviations gradually decrease for SST

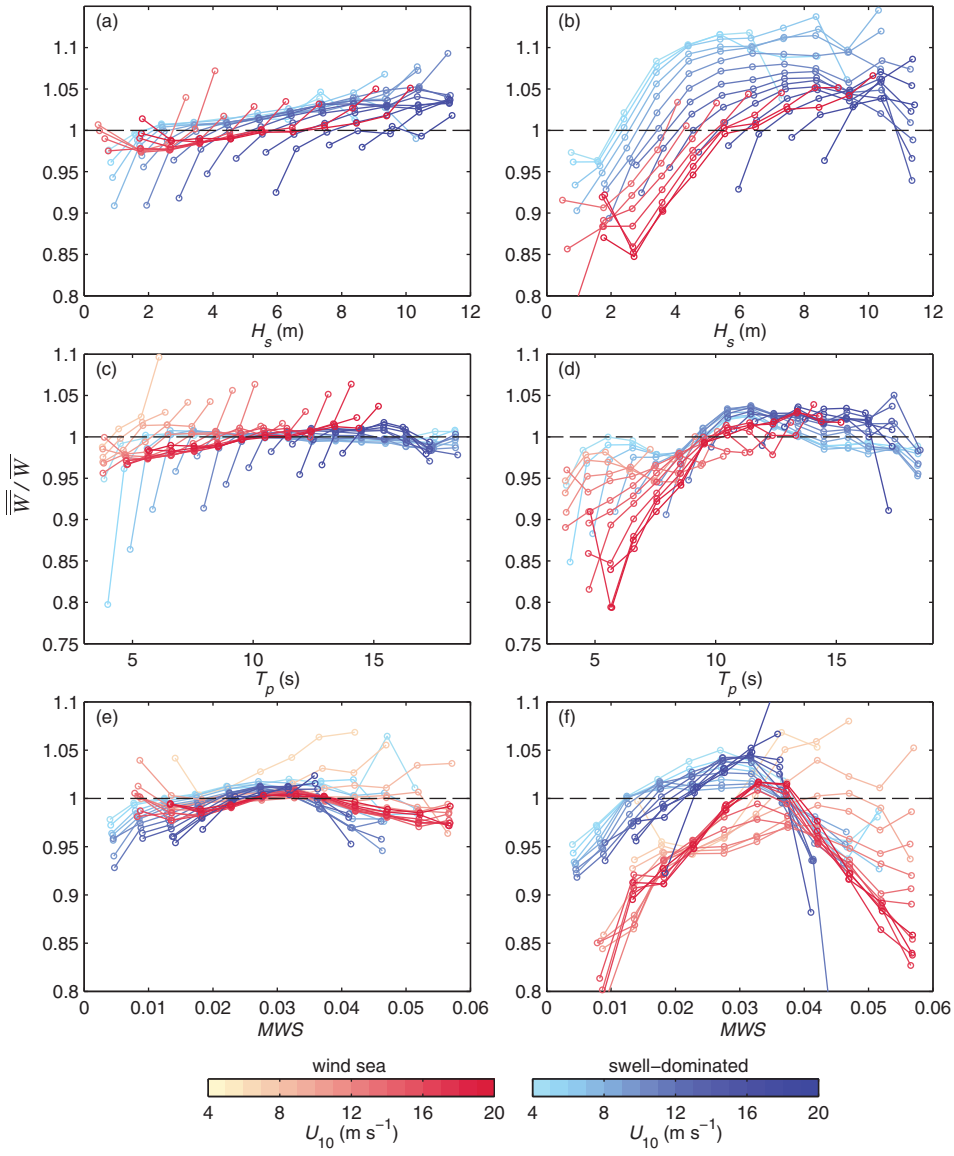

Figure 7. As Figure 6 but with data further classified into wind sea (yellow/red curves) and swell-dominated cases (blue curves).

ranging from 5 to 20°C. Whitecap fraction is suppressed by up to 25% for SST > 20°C.

[101] When plotted as a function of v_w (Figure 9d), the effect on normalized W_{37} is as expected from the results for SST. We stress the relatively small influence these factors have (no larger than 5%) on normalized W_{10} (Figure 9c). There is however slightly more uniform behavior between the trends in normalized W_{10} and W_{37} at the higher wind speeds (red), than that seen for SST.

[102] We explore the dependence of W upon air temperature and the air-sea temperature difference, ΔT, in Figure 10. The trends in both W_{10} and W_{37} for T_a (Figures 10a and 10b) are very similar to those found for SST; this is most likely due to near surface air temperature coming into (near) equilibrium with SST over much of the ocean.

[103] The influence of ΔT on W is less clear. The overall influence on W_{10} (Figure 10c) is again less than 5%; a slight peak in normalized W can be seen (at least for moderate to high wind speeds) just below $\Delta T = 0$, and a weak (5%) suppression for stronger unstable conditions. For W_{37} (Figure 10d), at moderate and high wind speeds, normalized W decreases as ΔT goes from unstable toward stable conditions. At the lower wind speeds, $\overline{\overline{W}}_{37}/\overline{W}_{37}$ shows enhancement for strongly unstable conditions, then falls off quickly as we go from unstable to near neutral conditions, but then increases slightly when ΔT becomes positive. In the most stable of conditions, normalized W_{37} is suppressed most at high wind speeds. The enhancement of normalized W_{37} is smaller in magnitude (~5% at 14 m s^{-1}) than its suppression (~10% at 14 m s^{-1}).

4.3. Relative Contribution of Forcing Factors

[104] The relative contribution of the different factors to variability in W is evaluated using PCA. We plot, for both W_{10} and W_{37}, the variance explained by the first Principal

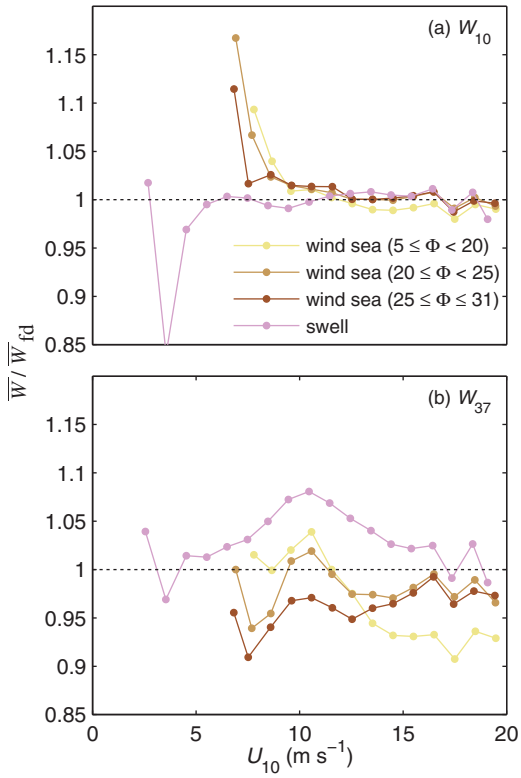

Figure 8. Ratio of wind speed averaged (a) W_{10} and (b) W_{37} to $\overline{W}_{fd}$ for swell and wind sea cases, with wind sea further classified by wave age.

Component (PC1) for wave and wind-wave variables (Figure 11a), and other environmental factors (Figure 11b). We consider all variables, including those which have an explicit dependence on wind speed—such as the two Reynolds numbers. The variables are ordered by the percent variance explained by PC1.

[105] The highest ranking variable is wind speed for both W_{10} and W_{37}. Two of the wind-wave variables (the breaking-wave and roughness Reynolds numbers) perform almost as well, with significantly higher scores than the other wind-wave variables considered. The next best performing wave variable is H_s, followed by Φ, and MWS. T_p accounts for only 50% of the variance of both W_{10} and W_{37}.

[106] T_a, SST, and ν_w all describe roughly the same percent variance. Notably, these three variables also show the biggest difference in variance explained by PC1 between W_{10} and W_{37}, accounting for ~4% more variance in W_{37} than in W_{10}. This supports the findings in section 4.2.3 that SST (or viscosity of water) has a more pronounced impact on W_{37} than on W_{10}. Note that this difference is not as large as one might expect because here we consider estimates covering almost the whole globe, whereas larger changes to W resulting from SST changes are probably confined to very warm waters (equatorial regions). In the case of the breaking wave Reynolds number and the roughness Reynolds number, variance explained by PC1 for W_{37} is slightly lower than that for W_{10}. Because both Reynolds numbers combine information on the wind field and wavefield, they may be better predictors of the variability of active foam

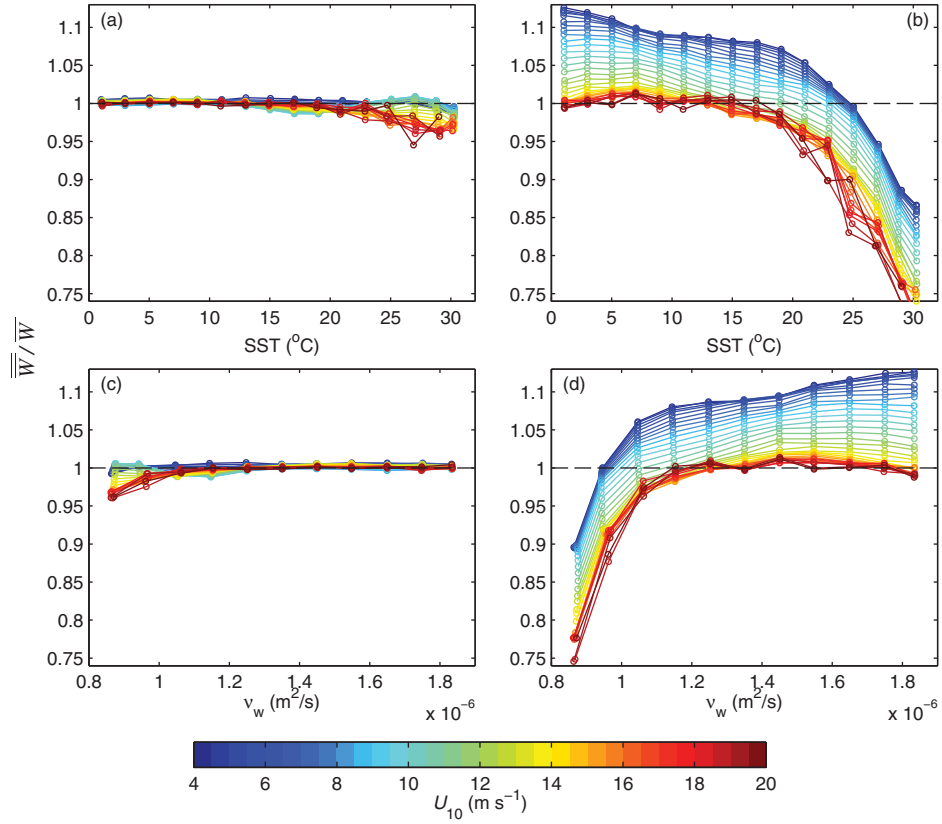

Figure 9. The dependence of (a and c) $\overline{\overline{W}}_{10}/\overline{W}_{10}$ and (b and d) $\overline{\overline{W}}_{37}/\overline{W}_{37}$ on (top) SST, and (bottom) viscosity of water.

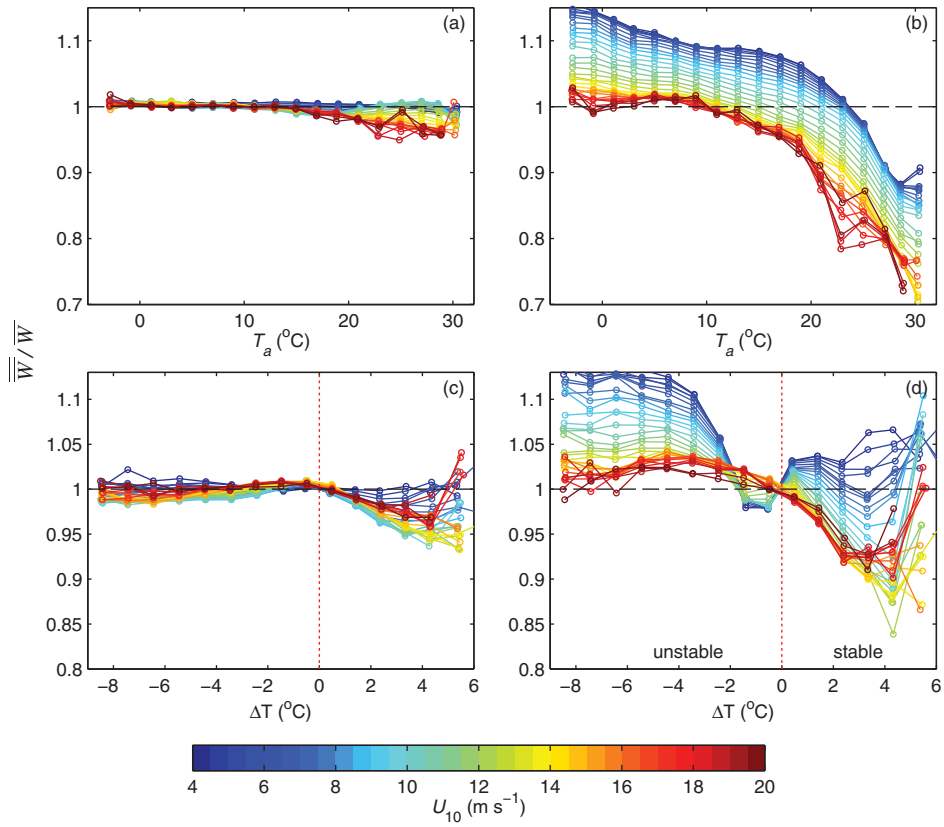

Figure 10. The dependence of (a and c) $\overline{\overline{W}}_{10}/\overline{W}_{10}$ and (b and d) $\overline{\overline{W}}_{37}/\overline{W}_{37}$ on (top) T_a and (bottom) ΔT.

(W_{10}), and not quite as successful when residual foam is included (W_{37}). The finding that the Reynolds numbers account for slightly less variance than wind speed alone is in stark contrast to a recent study of eddy covariance sea spray fluxes [*Norris et al.*, 2013], which found that a wave roughness Reynolds number explained up to twice the variance in the sea spray flux as wind speed alone. The slightly poorer performance of the Reynolds numbers here might result from inadequacies in model estimates of wave properties, the necessarily indirect estimate of u_*, or a degree of self-correlation between W and U_{10} introduced through the whitecap retrieval itself.

[107] When wind speed is included in the data sets (dashed lines), the ranking of the percent variance explained by PC1 is preserved, despite changes in the absolute values. In general, inclusion of wind speed lifts the variance explained by PC1—confirming that combining individual variables with wind speed is more effective in describing variability in W than the variable alone is. This is not the case for the two Reynolds numbers, for which inclusion of wind speed slightly lowers the percent variance explained by PC1; this is likely due to the dependence of both Reynolds numbers on wind speed through the friction velocity.

5. Discussion

5.1. Wind Speed Dependence

[108] The satellite retrieval of W_{10} is biased high with respect to the traditional $W(U_{10})$ parameterizations of *Monahan and O'Muircheartaigh* [1980] and *Callaghan et al.* [2008a] at low wind speeds, but falls below them for winds above about 10 m s^{-1}. W_{37} is even higher at low winds, but increases more slowly than W_{10}. The general behavior is similar to that reported by *Anguelova and Webster* [2006] in spite of substantial modifications to the retrieval

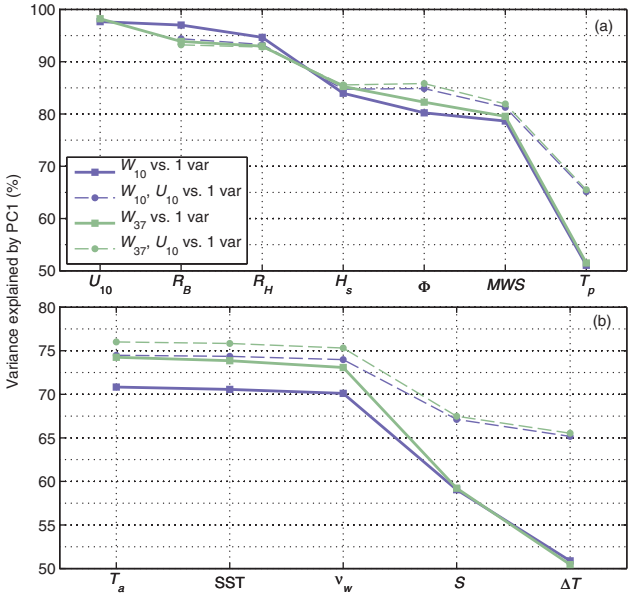

Figure 11. Percent variance explained by the first PC for data sets combining W with various other factors (solid lines), and the corresponding data sets when wind speed is included (dashed lines).

algorithm. Both W_{10} and W_{37} are closer to the parameterization of *Goddijn-Murphy et al*. [2011] —which uses satellite winds with the same in situ whitecap imagery used by *Callaghan et al*. [2008a] —than to the purely in situ functions. Indeed, the exponent of GM11 lies almost halfway between that of the W_{10} and W_{37} formulations presented here.

[109] Potential sources of relative bias between the different functions are systematic differences in the estimation of whitecap fraction and wind speed via different techniques, and from averaging over different ranges or probability distributions of secondary factors. We note that the best agreement between all the different functions is for winds in the range 5–10 m s^{-1}, those most commonly encountered over the ocean [*Ebuchi*, 1999]. Both the satellite winds and whitecap fraction estimates are spatial averages, while in situ winds are time averages at a single point and in situ whitecap fractions are joint time and spatial averages, albeit over a much more restricted area.

[110] The *Goddijn-Murphy et al*. [2011] function is even more strongly biased high (low) with respect to MM80 and Cal08 at low (high) wind speeds than W_{10}. This suggests that the differences between the different functions may depend as much, or more, on biases between the wind speed estimates as on the whitecap fraction measurements. A potentially significant factor here is that satellite winds are not estimates of the true 10 m wind speed, but of an equivalent neutral wind speed. There are also known issues such as the saturation of QuikSCAT for $U_{10} > 20$ m s^{-1} [*Quilfen et al*., 2007]. In situ winds are not necessarily without biases; ship-based measurements require correction of both their speed and effective altitude because of distortion of the air flow over the ship [*Yelland et al*., 2002; *Moat et al*., 2006], something only recognized relatively recently and not applied by earlier studies. Determining the correction is difficult however, and is not always undertaken even today—Cal08 do not correct their winds for flow distortion.

5.2. Secondary Factors

[111] Secondary factors may perturb the whitecap fraction from the mean for a given wind speed in several distinct ways: by changing the scale or frequency of wave breaking events, by modifying the bubble plume properties, and by modifying the surface foam properties. In all the cases studied, W_{37} (active and residual foam) shows a stronger response to secondary factors than does W_{10} (predominantly active whitecaps).

[112] Some care should be taken when interpreting Figures 6, 7, 9, and 10. The ratio of the observed W at a given value of both wind and secondary factor to the mean for each wind speed are shown. The means are calculated from the individual contributing values and are thus dependent on the probability distributions of the secondary factors. Offsets between the lines at different wind speeds may occur purely because of differences in these probability distributions at different wind speeds—for example, the range of significant wave heights observed is very different at high and low winds speeds, so that the mean W occurs at different values of H_s for different wind speeds. Relative trends in $\overline{W}/\overline{W}$ are thus more informative than the absolute values.

5.2.1. Influence of the Wavefield on W

[113] The results in Figures 6–8 relate the whitecap fraction to various measures of wave state. There exists considerable subtlety in the response of W to wave state, with W_{10} and W_{37} sometimes showing different behavior.

[114] Both W_{10} and W_{37} are generally suppressed in developing wind seas (low H_s and/or T_p) (Figures 7a–7d); the suppression is greatest when wind and waves are far from equilibrium as can be seen under conditions with moderate to high wind speed but very low T_p (Figure 7d). At low and moderate wind speeds, W peaks at $T_p \sim 11$ s; this peak shifts to higher T_p with increasing U_{10} for wind seas (Figures 7c and 7d).

[115] W tends to be largest when the wind and waves are in, or close to, equilibrium with the local wind. This enhancement close to wind-wave equilibrium is most clearly observed when *MWS* is used to define the wavefield; peak W occurs at $\sim$0.03, corresponding to waves in equilibrium with the wind. In wind sea conditions, the peak shifts to higher *MWS* (less well-developed waves) as the wind speed decreases. In wind seas at low wind speeds, W_{37} appears to continue to increase with *MWS*, but this may reflect a lack of data at sufficiently high *MWS*.

[116] When we compare W with that for a fully developed sea state for the local wind (Figure 8), we find no appreciable differences in W_{10} over much of the wind speed range. However, we again find a general trend of suppression of W_{37} in wind seas; at moderate wind speeds, largest suppression of W_{37} occurs in wind seas with highest wave age; at higher wind speeds largest suppression occurs in the youngest wind seas.

[117] The results above are consistent with recent studies showing enhancement of W in developed seas relative to that in under-developed seas [*Stramska and Petelski*, 2003; *Callaghan et al*., 2008b; *Goddijn-Murphy et al*., 2011], and of increasing W with wave age in wind seas [*Sugihara et al*., 2007].

[118] Using *MWS* to characterize the degree of wave development, we find suppression of W at a given wind speed in well-developed seas ($MWS < 0.03$) (Figures 7e and 7f); this suppression increases as the waves become increasingly overdeveloped. This picture is consistent with recent studies showing evidence for suppression of W in the presence of swell [*Sugihara et al*., 2007; *Callaghan et al*., 2008b].

[119] However, when we classify W estimates based on comparison of H_s and T_p with those expected for fully developed seas, we find that W_{37} is largest in swell-dominated seas (Figure 8b). This result may at first seem at odds with the results shown in Figures 7e and 7f. We must note the difference between use of *MWS* as an indicator of the wave state, and classification of W estimates based on comparing H_s and T_p to values expected for fully developed seas. The latter requires no information on local wind speed, and so cannot be judged as a definitive measure of the degree of wave development. In contrast, classification based on a comparison of H_s to H_{fd} and T_p to T_{fd} inherently considers the local wind speed. Different measures of wave development can give apparently contradictory impressions; this results from the partial picture provided by averaging different subsets of the data, suggesting the need for

more detailed information on wave spectra to fully resolve the wave influences on whitecap fraction.

[120] For wind sea dominated conditions, the increase in W with wave state is readily interpreted as resulting simply from larger waves and consequently either larger individual breakers or more frequent breaking events. For swell-dominated conditions, the behavior is more complicated with W having a more or less distinct peak at some mid-range of wave state, decreasing for both less well and better developed wave states. We speculate that this results from changes in wave-wave interactions between the wind sea and swell as a function of the difference between their respective wavelengths.

[121] Both wind waves and swell are dispersive, and grow and break suddenly as a consequence of wave-wave interactions as individual waves pass through a wave group [*Donelan and Pierson*, 1987]. The steepening of waves during such interactions is greatest when the wavelengths are similar, decreasing as the difference in wavelength increases. Swell-dominated cases where the swell and wind waves are similar in wavelength would thus be expected to enhance wave breaking, while those where the wavelengths were very different would not. We note that W_{10} follows this pattern with T_p but not with H_s; we attribute this to the fact that T_p provides a better measure of separation on wind sea and swell scales, while the H_s results are averaged over a range of wave and swell scales combined.

[122] We have considered the success of several wind-wave and wave variables in accounting for variability in W. Of these, the two Reynolds numbers perform best. It has been shown previously that the primary contribution to wave breaking and resulting whitecaps comes from the high frequency components of the wave spectrum, and not the dominant waves [*Dulov et al*., 2002; *Gemmrich et al*., 2008; *Plant*, 2012]. Therefore, the success of wind-wave variables in accounting for variability in W may be improved with use of wave measurements describing the wind sea part of the spectrum only, e.g., the peak wave period for wind waves, rather than peak wave period of the total spectrum. This hypothesis could be tested with expansion of the database to include wave measures quantifying a partitioned spectrum.

5.2.2. SST Effects

[123] Both normalized W_{10} and normalized W_{37} show a clear decrease in whitecap fraction for SSTs greater than about 15–20°C; the suppression is much stronger for normalized W_{37}. The findings could be explained following the argument of *Monahan et al*. [1983], namely that rise times of bubbles are longer in colder waters, resulting in longer whitecap lifetimes and hence greater values of W under the same meteorological conditions. However, *Leifer et al*. [2000] have shown that for clean bubbles the SST effect on the bubble rise velocity is size dependent. This suggests that SST would influence the whitecap fraction not just through the decay rate, but also by changing the bubble size distribution that contributes to the surface foam layer. Because *Anguelova and Gaiser* [2011, 2013] have shown that foam emissivity and thus T_B due to whitecaps depends on the void fraction and thickness of the foam layers, one could expect W_{10} and W_{37} to be sensitive to such an influence. Studies of such intriguing connections would require data on bubble size distributions from regions with different seawater temperatures—this is only possible for in situ studies, not satellite based retrievals.

[124] Our results for W_{37} could be further explained by a reduction in the decay time of residual foam patches with increasing SST [*Bortkovskii and Novak*, 1993], while those for W_{10} remain harder to explain. The relatively flat response to SST below 15–20°C is consistent with *Stramska and Petelski* [2003], who found no SST response between 2 and 13°C.

[125] Another possibility is that the observed SST dependence is a result of a spatial correlation between SST and some other factor affecting whitecap properties such as the concentration of organic surfactants in the surface water. *Callaghan et al*. [2013] confirmed that the presence of surfactants acts to stabilize surface bubbles and so increase whitecap decay times. In the open ocean, the primary source of natural surfactant compounds are phytoplankton exudates, which can be transported to the surface through diffusion and via rising bubbles [*Žutić et al*., 1981]. Surfactant concentrations tend to be higher in cooler waters where nutrients are more plentiful and primary production is higher. This inverse correlation between SST and phytoplankton concentration [*Falkowski et al*., 1998; *McClain et al*., 2004] might thus be expected to contribute to a relative reduction in the lifetime of residual foam in warm waters. W_{10} might be influenced by surfactant concentration if the retrieval includes some fraction of the residual foam, or if surfactants modify the bubble properties in active breakers sufficiently to affect the retrieval algorithm. Finally, we cannot entirely exclude the possibility that uncertainty in the models used in the W algorithm (section 3.1.1) might contribute to the observed temperature dependence.

[126] The impact of viscosity largely reflects that of SST, although there is a little less scatter, particularly for W_{37}; this may result from the inclusion of salinity as well as temperature.

5.2.3. Atmospheric Stability Effects

[127] The air temperature dependence of W_{10} and W_{37} follows that of the SST dependence. Since air and water temperatures do not usually differ by more than a few degrees Celsius over much of the ocean [*Kara et al*., 2007], it is likely that results are largely due to the SST dependence.

[128] We find W_{10} is largest for weakly unstable conditions at most wind speeds; there is little change for $\Delta T < -3$°C, but a decrease with increasing stability. W_{37} displays even more complex behavior; for U_{10} above about 13 m s^{-1}, the behavior is similar to that for W_{10}, with slight decrease for stronger instabilities and a greater decrease with increasing stability. At low wind speeds, W_{37} is generally lowest for weakly unstable conditions, with largest enhancement of W for the most unstable conditions.

[129] Previous studies have found an increase in W for unstable conditions [*Monahan and O'Muircheartaigh*, 1986; *Wu*, 1988; *Monahan and Woolf*, 1988]. This is plausibly explained by an increase in u_* at a given wind speed because of the additional turbulence generated by convection. Some caution is needed when interpreting our results, however; the satellite winds used here are not true local values, but the equivalent wind under neutral conditions. Scatterometer backscatter depends on short surface

waves, which respond rapidly to the local wind stress, rather than wind speed, and are calibrated to give the equivalent neutral wind that would provide the same wind stress [*Tang and Liu*, 1996]. Thus our measurements should not be expected to exhibit the same wind speed/stress dependence on stability as in situ measurements. The stability dependence of W_{10} and W_{37} must thus have some other cause.

[130] We speculate that one possible cause is a change in the spatial distribution of wind stress with stability within the satellite footprint. Under unstable conditions, the superposition of large scale convective motions on the mean wind may lead to highly variable local surface winds, and wind stress, due to convergent flow at the base of updrafts at scales much smaller than the footprint of the brightness temperature measurement. This will lead to spatially variable whitecap formation, and because whitecap fraction is a highly nonlinear function of the local wind, the spatially averaged W will be higher than that for the same spatially averaged mean wind. The nature of the spatial variability will change with both the strength of the instability and with the mean wind speed, and may include more or less randomly distributed, isolated thermal plumes, organized cellular convection with open or closed cells, and linearly organized boundary layer rolls.

5.3. Radiometric Frequency Dependence of W Estimates

[131] The operational radiometric frequency is an important aspect of satellite estimates of whitecap fraction, with different frequencies able to discriminate, at least approximately, between foam layers depending on their thickness (section 3.1.2). Our results show unambiguously that wind speed and secondary factors affect W_{10} and W_{37} differently.

[132] Importantly, these differences can be plausibly explained with different influences of the secondary factors on foam layers associated with different whitecap lifetime stages. This lends support to the notion that W_{10} and W_{37} represent different mixes of active and residual whitecaps. This is also an independent confirmation of the conclusions regarding the frequency sensitivity to foam layer thicknesses which *Anguelova and Gaiser* [2011] obtained on the basis of purely physical considerations. Whitecap fraction is currently used to parameterize numerous bubble-dependent air-sea processes, but it is expected that these parameterizations could be improved through use of measures of W that discriminate between active breakers and residual foam. As such, microwave measurements of whitecap fraction could prove beneficial to parameterization of such processes.

6. Conclusions

[133] We have presented an analysis of whitecap fraction estimated from satellite-based radiometric observations at frequencies of 10 GHz (W_{10}) and 37 GHz (W_{37}). The retrieval provides a several order of magnitude increase in the number of individual estimates of W compared to historical in situ data, as well as global coverage. Using collocated and concurrent measurements of a variety of physically relevant quantities in addition to wind speed, we have investigated the influence of secondary factors on whitecap fraction.

[134] Variability in W is smaller for active whitecaps (W_{10}) and larger for total whitecap fraction which includes both active and residual whitecaps (W_{37}). Within each secondary dependence, the effect of the secondary parameter is, in most cases, stronger at higher winds than at lower, supporting the findings from the in situ studies of *Callaghan et al*. [2008a] and *Goddijn-Murphy et al*. [2011].

[135] Wind speed alone accounts for most of the variability in both W_{10} and W_{37}. At a given wind speed, variability due to secondary factors is more pronounced for W_{37} than for W_{10} with W_{37} changing by as much as 20% when wave height, wave period, or the mean wave slope are considered, and by up to 25% when SST or T_a are considered. This clear SST trend is largely due to the strong suppression of W_{37} in high SST (low viscosity) waters.

[136] The influence of the degree of wave development has been assessed. We conclude that at a given wind speed, W is lower in conditions of a developing sea compared with a fully developed sea. The effect on W of the wave state in swell conditions is more complex; these findings require further investigation with more detailed wave measurements including directional information, and ideally, measures quantifying the wind sea and swell parts of the wave spectrum separately.

[137] Principal component analysis has been used to assess the success of wind speed and secondary forcing parameters in accounting for variability in W. Two Reynolds number parameters—combining measures of wind speed, wave height or period, and viscosity—perform almost as well as wind speed alone. Different measures of the degree of wave development (wave age and mean wave slope) can account for between 80% and 85% of variability in W. The first principal component for air temperature, SST, and the viscosity of water account for roughly the same level of variance in W; 71% for W_{10} and 74% for W_{37}.

[138] Estimation of satellite-derived whitecap fraction is dependent upon the retrieval wavelength. From an analysis of the influence of secondary forcings on W, we conclude that much of the variability in foam layer might be due to the behavior of the thinner, decaying foam patches, variability that is not captured by the retrieval using the 10 GHz channel.

[139] The utility of a database of improved, satellite-based estimates of W could be augmented by adding data sets for directional wave spectra, currents (speed and direction), and proxies for surfactants such as ocean color, chlorophyll a, or oceanic primary production. The database could be further enforced when combined, on regional scales, with data for underwater bubble plumes and their characteristics or sea spray production rates. All these additional data can be used to more specifically determine causes for variability in W.

[140] Whilst work to improve the W algorithm is ongoing, significant changes to the results presented here are unlikely.

[141] **Acknowledgments.** We express our thanks to the WindSat team at the Naval Research Laboratory, Washington, District of Columbia. D. S. and I. M. B. are supported by NERC grant NE/H004238/1. M. D. A. is supported by the Office of Naval Research, NRL Program element

61153N, work units WU 8967 and WU 4500. We acknowledge the comments and helpful suggestions of three anonymous reviewers which have greatly improved the structure and content of this paper.

References

Andreae, M., and D. Rosenfeld (2008), Aerosol-cloud-precipitation interactions. Part 1: The nature and sources of cloud-active aerosols, *Earth Sci. Rev.*, *89*(1–2), 13–41, doi:10.1016/j.earscirev.2008.03.001.

Andreas, E. L. (1995), The temperature of evaporating sea spray droplets, *J. Atmos. Sci.*, *52*, 852–862, doi:10.1175/1520-0469(1995)052⟨0852:TTOESS⟩2.0.CO;2.

Andreas, E. L., and K. A. Emanuel (2001), Effects of sea spray on tropical cyclone intensity, *J. Atmos. Sci.*, *58*(24), 3741–3751, doi:10.1175/1520-0469(2001)058⟨3741:EOSSOT⟩2.0.CO;2.

Andreas, E. L., and E. C. Monahan (2000), The role of whitecap bubbles in air-sea heat and moisture exchange, *J. Phys. Oceanogr.*, *30*(2), 433–442, doi:10.1175/1520-0485(2000)030⟨0433:TROWBI⟩2.0.CO;2.

Andreas, E. L., J. B. Edison, E. Monahan, M. P. Rouault, and S. D. Smith (1995), The spray contribution to net evaporation from the sea: A review of recent progress, *Boundary Layer Meteorol.*, *72*(1), 3–52, doi:10.1007/BF00712389.

Andreas, E. L., P. O. G. Persson, and J. E. Hare (2008), A bulk turbulent air-sea flux algorithm for high-wind, spray conditions, *J. Phys. Oceanogr.*, *38*(7), 1581–1596, doi:10.1175/2007JPO3813.1.

Anguelova, M. D., and P. W. Gaiser (2011), Skin depth at microwave frequencies of sea foam layers with vertical profile of void fraction, *J. Geophys. Res.*, *116*, C11002, doi:10.1029/2011JC007372.

Anguelova, M. D., and P. W. Gaiser (2013), Microwave emissivity of seafoam layers with vertical profile of dielectric properties, *Remote Sens. Environ.*, *139*, 81–96, doi:10.1016/j.rse.2013.07.017.

Anguelova, M. D., and F. Webster (2006), Whitecap coverage from satellite measurements: A first step toward modeling the variability of oceanic whitecaps, *J. Geophys. Res.*, *111*, C03017, doi:10.1029/2005JC003158.

Anguelova, M. D., J. P. Bobak, W. E. Asher, D. J. Dowgiallo, B. I. Moat, R. W. Pascal, and M. J. Yelland (2009), Validation of satellite-based estimates of whitecap coverage: Approaches and initial results, paper presented at 16th Conference on Air Sea Interaction, Am. Meteorol. Soc., Phoenix, Ariz. [Available at https://ams.confex.com/ams/pdfpapers/143665.pdf.].

Anguelova, M. D., M. Bettenhausen, W. Johnston, and P. W. Gaiser (2010), First extensive whitecap database and its use to study whitecap fraction variability, paper presented at 17th Conference on Air Sea Interaction, Am. Meteorol. Soc., Annapolis, Md.

Bettenhausen, M., C. Smith, R. Bevilacqua, N. Wang, P. Gaiser, and S. Cox (2006), A nonlinear optimization algorithm for WindSat wind vector retrievals, *IEEE Trans. Geosci. Remote Sens.*, *44*(3), 597–610, doi:10.1109/TGRS.2005.862504.

Blanchard, D. (1963), The electrification of the atmosphere by particles from bubbles in the sea, *Prog. Oceanogr.*, *1*, 73–112.

Blanchard, D. (1983), The production, distribution and bacterial enrichment of the sea-salt aerosol, in *Air-Sea Exchange of Gases and Particles*, edited by P. Liss and G. Slinn, pp. 407–454, Springer, New York.

Bobak, J. P., W. E. Asher, D. J. Dowgiallo, and M. D. Anguelova (2011), Aerial radiometric and video measurements of whitecap coverage, *IEEE Trans. Geosci. Remote Sens.*, *49*(6), 2183–2193, doi:10.1109/TGRS.2010.2103565.

Bortkovskii, R. S., and V. A. Novak (1993), Statistical dependencies of sea state characteristics on water temperature and wind-wave age, *J. Mar. Syst.*, *4*(2), 161–169.

Bourassa, M. A., D. G. Vincent, and W. L. Wood (2001), A sea state parameterization with capillary waves and non-arbitrary wave age, *J. Phys. Oceanogr.*, *31*, 2840–2851, doi:10.1175/1520-0485(2001)031⟨2840:ASPWN⟩2.0.CO;2.

Callaghan, A., G. de Leeuw, L. Cohen, and C. D. O'Dowd (2008a), Relationship of oceanic whitecap coverage to wind speed and wind history, *Geophys. Res. Lett.*, *35*, L23609, doi:10.1029/2008GL036165.

Callaghan, A. H. (2013), An improved whitecap timescale for sea spray aerosol production flux modelling using the discrete whitecap method, *J. Geophys. Res. Atmos.*, *118*, 9997–10,010, doi:10.1002/jgrd.50768.

Callaghan, A. H., and M. White (2009), Automated processing of sea surface images for the determination of whitecap coverage, *J. Atmos. Oceanic Technol.*, *26*(2), 383–394, doi:10.1175/2008JTECHO634.1.

Callaghan, A. H., G. B. Deane, and M. D. Stokes (2008b), Observed physical and environmental causes of scatter in whitecap coverage values in a fetch-limited coastal zone, *J. Geophys. Res.*, *113*, C05022, doi:10.1029/2007JC004453.

Callaghan, A. H., G. B. Deane, M. D. Stokes, and B. Ward (2012), Observed variation in the decay time of oceanic whitecap foam, *J. Geophys. Res.*, *117*, C09015, doi:10.1029/2012JC008147.

Callaghan, A. H., G. B. Deane, and D. M. Stokes (2013), Two regimes of laboratory whitecap foam decay: Bubble-plume controlled and surfactant stabilized, *J. Phys. Oceanogr.*, *43*, 1114–1126, doi:10.1175/JPO-D-12–0148.1.

Cardone, V. J. (1969), Specification of the wind distribution in the marine boundary layer for wave forecasting, Tech. Rep. 69-1, 131 pp., Geophys. Sci. Lab., New York Univ., New York.

Carter, D. J. T. (1982), Prediction of wave height and period for a constant wind velocity using the JONSWAP results, *Ocean Eng.*, *9*(1), 17–33.

Chelton, D. B., and M. H. Freilich (2005), Scatterometer-based assessment of 10-m wind analyses from the operational ECMWF and NCEP numerical weather prediction models, *Mon. Weather Rev.*, *133*(2), 409–429, doi:10.1175/MWR-2861.1.

Chen, G., B. Chapron, R. Ezraty, and D. Vandemark (2002), A global view of swell and wind sea climate in the ocean by satellite altimeter and scatterometer, *J. Atmos. Oceanic Technol.*, *19*(11), 1849–1859, doi:10.1175/1520-0426(2002)019⟨1849:AGVOSA⟩2.0.CO;2.

de Leeuw, G., E. L. Andreas, M. D. Anguelova, C. W. Fairall, E. R. Lewis, C. O'Dowd, M. Schulz, and S. E. Schwartz (2011), Production flux of sea spray aerosol, *Rev. Geophys.*, *49*, RG2001, doi:10.1029/2010RG000349.

Deane, G. B., and M. D. Stokes (2002), Scale dependence of bubble creation mechanisms in breaking waves, *Nature*, *418*(6900), 839–844, doi:10.1038/nature00967.

Donelan, M. A., and W. J. Pierson Jr. (1987), Radar scattering and equilibrium ranges in wind-generated waves with application to scatterometry, *J. Geophys. Res.*, *92*(C5), 4971–5029.

Dulov, V. A., V. N. Kudryavtsev, and A. N. Bol'Shakov (2002), A field study of whitecap coverage and its modulations by energy containing surface waves, in *Gas Transfer at Water Surfaces*, edited by M. A. Donelan et al., pp. 187–192, AGU, Washington, D. C.

Ebuchi, N. (1999), Statistical distribution of wind speeds and directions globally observed by NSCAT, *J. Geophys. Res.*, *104*(C5), 11,393–11,403.

Fairall, C. W., E. F. Bradley, J. E. Hare, A. A. Grachev, and J. B. Edson (2003), Bulk parameterization of air-sea fluxes: Updates and verification for the COARE algorithm, *J. Clim.*, *16*(4), 571–591, doi:10.1175/1520-0442(2003)016⟨0571:BPOASF⟩2.0.CO;2.

Falkowski, P. G., R. T. Barber, and V. Smetacek (1998), Biogeochemical controls and feedbacks on ocean primary production, *Science*, *281*(5374), 200–206, doi:10.1126/science.281.5374.200.

Frouin, R., S. F. Iacobellis, and P. Y. Deschamps (2001), Influence of oceanic whitecaps on the global radiation budget, *Geophys. Res. Lett.*, *28*(8), 1523–1526, doi:10.1029/2000GL012657.

Gaiser, P. W., et al. (2004), The WindSat spaceborne polarimetric microwave radiometer: Sensor description and early orbit performance, *IEEE Trans. Geosci. Remote Sens.*, *42*(11), 2347–2361, doi:10.1109/TGRS.2004.836867.

Garrett, W. D. (1967), Stabilization of air bubbles at the air-sea interface by surface-active material, *Deep Sea Res. Oceanogr. Abstr.*, *14*(6), 661–672, doi:10.1016/S0011–7471(67)80004-4.

Gemmrich, J. R., M. L. Banner, and C. Garrett (2008), Spectrally resolved energy dissipation rate and momentum flux of breaking waves, *J. Phys. Oceanogr.*, *38*(6), 1296–1312, doi:10.1175/2007JPO3762.1.

Goddijn-Murphy, L., D. K. Woolf, and A. H. Callaghan (2011), Parameterizations and algorithms for oceanic whitecap coverage, *J. Phys. Oceanogr.*, *41*(4), 742–756, doi:10.1175/2010JPO4533.1.

Gordon, H. R., and M. Wang (1994), Influence of oceanic whitecaps on atmospheric correction of ocean-color sensors, *Appl. Opt.*, *33*(33), 7754–7763, doi:10.1364/AO.33.007754.

Hanley, K. E., S. E. Belcher, and P. P. Sullivan (2010), A global climatology of wind-wave interaction, *J. Phys. Oceanogr.*, *40*(6), 1263–1282, doi:10.1175/2010JPO4377.1.

Hasselmann, S., et al. (1988), The WAM model: A third generation ocean wave prediction model, *J. Phys. Oceanogr.*, *18*, 1775–1810.

Haywood, J. M., V. Ramaswamy, and B. J. Soden (1999), Tropospheric aerosol climate forcing in clear-sky satellite observations over the oceans, *Science*, *283*(5406), 1299, doi:10.1126/science.283.5406.1299.

Holthuijsen, L. H. (2007), *Waves in Oceanic and Coastal Waters*, Cambridge Univ. Press, Cambridge, U. K., doi:10.1029/2012JC007983.

Jessup, A., C. J. Zappa, and H. Yeh (1997), Defining and quantifying g wave breaking with infrared imagery, *J. Geophys. Res.*, *102*(C10), 23,145–23,153.

Johnson, J. T. (2006), An efficient two-scale model for the computation of thermal emission and atmospheric reflection from the sea surface, *IEEE Trans. Geosci. Remote Sens.*, *44*(3), 560–568, doi:10.1109/TGRS.2005.855999.

Kara, A., A. Wallcraft, and M. Bourassa (2008), Air-sea stability effects on the 10 m winds over the global ocean: Evaluations of air-sea flux algorithms, *J. Geophys. Res.*, *113*, C04009, doi:10.1029/2007JC004324.

Kara, A. B., H. E. Hurlburt, and W.-Y. Loh (2007), Which near-surface atmospheric variable drives air–sea temperature differences over the global ocean?, *J. Geophys. Res.*, *112*, C05020, doi:10.1029/2006JC003833.

Kleiss, J. M., and W. K. Melville (2011), The analysis of sea surface imagery for whitecap kinematics, *J. Atmos. Oceanic Technol.*, *28*(2), 219–243, doi:10.1175/2010JTECHO744.1.

Koepke, P. (1984), Effective reflectance of oceanic whitecaps, *Appl. Opt.*, *23*(11), 1816–1824, doi:10.1364/AO.23.001816.

Lafon, C., J. Piazzola, P. Forget, and S. Despiau (2007), Whitecap coverage in coastal environment for steady and unsteady wave field conditions, *J. Mar. Syst.*, *66*(1–4), 38–46, doi:10.1016/j.jmarsys.2006.02.013.

Large, W. G., and S. Pond (1981), Open ocean momentum flux measurements in moderate to strong winds, *J. Phys. Oceanogr.*, *11*(3), 324–336, doi:10.1175/1520-0485(1981)011⟨0324:OOMFMI⟩2.0.CO;2.

Leifer, I., R. K. Patro, and P. Bowyer (2000), A study on the temperature variation of rise velocity for large clean bubbles, *J. Atmos. Oceanic Technol.*, *17*(10), 1392–1402, doi:10.1175/1520-0426(2000)017⟨1392:ASOTTV⟩2.0.CO;2.

Lewis, E., and S. Schwartz (2004), *Sea Salt Aerosol Production: Mechanisms, Methods, Measurements and Models: A Critical Review*, AGU, Washington, D. C., doi:10.1029/GM152.

Massel, S. R. (2007), *Ocean Waves Breaking and Marine Aerosol Fluxes, Atmospheric and Oceanographic Sciences Library*, vol. *38*, Springer, New York, doi:10.1007/978-0-387–69092-6.

McClain, C. R., G. C. Feldman, and S. B. Hooker (2004), An overview of the SeaWiFS project and strategies for producing a climate research quality global ocean bio-optical time series, *Deep Sea Res., Part II*, *51*(1), 5–42, doi:10.1016/j.dsr2.2003.11.001.

Moat, B. I., M. J. Yelland, and A. F. Molland (2006), Quantifying the airflow distortion over merchant ships. Part II: Application of the model results, *J. Atmos. Oceanic Technol.*, *23*(3), 351–360, doi:10.1175/JTECH1859.1.

Moat, B. I., M. J. Yelland, and R. W. Pascal (2009), Oceanic whitecap coverage measured during UK-SOLAS cruises, paper presented at 16th Conference on Air Sea Interaction, Am. Meteorol. Soc., Phoenix, 15–19 Jan.

Monahan, E., C. Fairall, K. Davidson, and P. Boyle (1983), Observed interrelations between 10m winds, ocean whitecaps and marine aerosols, *Q. J. R. Meteorol. Soc.*, *109*(460), 379–392, doi:10.1002/qj.49710946010.

Monahan, E. C. (1971), Oceanic whitecaps, *J. Phys. Oceanogr.*, *1*, 139–144, doi:10.11751520-0485(1971)001⟨0139:OW⟩2.0.CO;2.

Monahan, E. C., and H. G. Dam (2001), Bubbles: An estimate of their role in the global oceanic flux of carbon, *J. Geophys. Res.*, *106*(C5), 9377–9383, doi:10.1029/2000JC000295.

Monahan, E. C., and M. Lu (1990), Acoustically relevant bubble assemblages and their dependence on meteorological parameters, *IEEE J. Oceanic Eng.*, *15*(4), 340–349, doi:10.1109/48.103530.

Monahan, E. C., and I. G. O'Muircheartaigh (1980), Optimal power-law description of oceanic whitecap coverage dependence on wind speed, *J. Phys. Oceanogr.*, *10*, 2094–2099, doi:10.1175/1520-0485(1980)010⟨2094:OPLDOO⟩2.0.CO;2.

Monahan, E. C., and I. G. O'Muircheartaigh (1986), Whitecaps and the passive remote sensing of the ocean surface, *Int. J. Remote. Sens.*, *7*(5), 627–642, doi:10.1080/01431168608954716.

Monahan, E. C., and M. C. Spillane (1984), The role of oceanic whitecaps in air-sea gas exchange, in *Gas Transfer at Water Surfaces*, edited by M. A. Donelan et al., pp. 495–503, Springer, New York.

Monahan, E. C., and D. Woolf (1988), Comments on ''Variations of whitecap coverage with wind stress and water temperature,'' *J. Phys. Oceanogr.*, *19*, 706–709, doi:10.1175/1520-0485(1989)019⟨0706:COOWCW⟩2.0.CO;2.

Monahan, E. C., and C. R. Zietlow (1969), Laboratory comparisons of fresh-water and salt-water whitecaps, *J. Geophys. Res.*, *74*(28), 6961–6966, doi:10.1029/JC074i028p06961.

Norris, S. J., I. M. Brooks, and D. J. Salisbury (2013), A wave roughness Reynolds number parameterization of the sea-spray source flux, *Geophys. Res. Lett.*, *40*, 4415–4419, doi:10.1002/grl.50795.

O'Dowd, C., M. C. Facchini, F. Cavalli, D. Ceburnis, M. Mircea, S. Decesari, S. Fuzzi, Y. J. Yoon, and J. P. Putaud (2004), Biogenically driven organic contribution to marine aerosol, *Nature*, *431*(7009), 676–680, doi:10.1038/nature02959.

O'Dowd, C., B. Langmann, S. Varghese, C. Scannell, D. Ceburnis, and M. Facchini (2008), A combined organic-inorganic sea-spray source function, *Geophys. Res. Lett.*, *35*, L01801, doi:10.1029/2007GL030331.

Peltzer, R. D., and O. M. Griffin (1987), The stability and decay of foam in sea water, *Ocean Phys. Eng.*, *12*(2), 101–126.

Pierson, W. J., G. Neumann, and R. W. James (1955), *Practical Methods for Observing and Forecasting Ocean Waves by Means of Wave Spectra and Statistics*, 284 pp., U.S. Navy Hydrographic Office H.O. Pub 603, Washington, D. C.

Plant, W. J. (2012), Whitecaps in deep water, *Geophys. Res. Lett.*, *39*, L16601, doi:10.1029/2012GL052732.

Pounder, C. (1986), Sodium chloride and water temperature effects on bubbles, in *Oceanic Whitecaps and Their Role in Air-Sea Exchange Processes*, edited by E. C. Monahan and G. MacNiocaill, pp. 278–278, D. Reidel, Dordrecht, the Netherlands, Springer, Netherlands.

Preisendorfer, R., and C. Mobley (1988), *Principal Component Analysis in Meteorology and Oceanography*, vol. *425*, Elsevier, New York.

Quilfen, Y., C. Prigent, B. Chapron, A. A. Mouche, and N. Houti (2007), The potential of QuikSCAT and WindSat observations for the estimation of sea surface wind vector under severe weather conditions, *J. Geophys. Res.*, *112*, C09023, doi:10.1029/2007JC004163.

Rose, L., W. Asher, S. Reising, P. Gaiser, K. St Germain, D. Dowgiallo, K. Horgan, G. Farquharson, and E. Knapp (2002), Radiometric measurements of the microwave emissivity of foam, *IEEE Trans. Geosci. Remote Sens.*, *40*(12), 2619–2625, doi:10.1109/TGRS.2002.807006.

Scott, J. C. (1986), The effect of organic films on water surface motions, in *Oceanic Whitecaps and Their Role in Air-Sea Exchange Processes*, edited by Monahan, E. C. and MacNiocaill, G., pp. 159–165, D. Reidel, Dordrecht, the Netherlands, doi:10.1007/978-94-009–4668-2_15.

Smith, P. (1988), The emissivity of sea foam at 19 and 37 GHz, *IEEE Trans. Geosci. Remote Sens.*, *26*(5), 541–547, doi:10.1109/36.7679.

Spillane, M. C., E. C. Monahan, P. A. Bowyer, D. M. Doyle, and P. J. Stabeno (1986), Whitecaps and global fluxes, in *Oceanic Whitecaps and Their Role in Air-Sea Exchange Processes*, edited by E. C. Monahan and G. MacNiocaill, pp. 209–218, D. Reidel, Dordrecht, the Netherlands, Springer, New York, doi:10.1007/978-94-009–4668-2_19.

Stramska, M., and T. Petelski (2003), Observations of oceanic whitecaps in the north polar waters of the Atlantic, *J. Geophys. Res.*, *108*(C3), 3086, doi:10.1029/2002JC001321.

Sugihara, Y., H. Tsumori, T. Ohga, H. Yoshioka, and S. Serizawa (2007), Variation of whitecap coverage with wave-field conditions, *J. Mar. Syst.*, *66*(1–4), 47–60, doi:10.1016/j.jmarsys.2006.01.014.

Tang, W., and W. T. Liu (1996), *Equivalent Neutral Wind*, Publ. 96017, Jet Propul. Lab., Pasadena, Calif.

Toba, Y., and M. Chaen (1973), Quantitative expression of the breaking of wind waves on the sea surface, *Rec. Oceanogr. Works Jpn.*, *12*(1), 11.

Toba, Y., and M. Koga (1986), A parameter describing overall conditions of wave breaking, whitecapping, sea-spray production, and wind stress, in *Oceanic Whitecaps and Their Role in Air-Sea Exchange Processes*, edited by E. Monahan and G. Niocaill, pp. 37–48, Springer, New York, doi:10.1007/978-94-009–4668-2_4.

Ulaby, F., R. Moore, and A. Fung (1981), Microwave remote sensing: Active and passive, in *Microwave Remote Sensing Fundamentals and Radiometry*, vol. 1, Addison-Wesley, Reading, Mass.

Vignati, E., et al. (2010), Global scale emission and distribution of sea-spray aerosol: Sea-salt and organic enrichment, *Atmos. Environ.*, *44*(5), 670–677, doi:10.1016/j.atmosenv.2009.11.013.

Wanninkhof, R., W. E. Asher, D. T. Ho, C. Sweeney, and W. R. McGillis (2009), Advances in quantifying air-sea gas exchange and environmental forcing, *Ann. Rev. Mar. Sci.*, *1*, 213–244, doi:10.1146/annurev.marine.010908.163742.

Wentz, F. (1997), A well-calibrated ocean algorithm for special sensor microwave/imager, *J. Geophys. Res.*, *102*(C4), 8703–8718, doi:10.1029/96JC01751.

Wentz, F. J. (1983), A model function for ocean microwave brightness temperatures, *J. Geophys. Res.*, *88*(C3), 1892–1908, doi:10.1029/JC088iC03p01892.

Wentz, F. J. (1992), Measurement of oceanic wind vector using satellite microwave radiometers, *IEEE Trans. Geosci. Remote Sens.*, *30*(5), 960–972, doi:10.1109/36.175331.

Whitlock, C. H., D. S. Bartlett, and E. A. Gurganus (1982), Sea foam reflectance and influence on optimum wavelength for remote sensing of ocean aerosols, *Geophys. Res. Lett.*, *9*(6), 719–722, doi:10.1029/GL009i006p00719.

Woolf, D. (1997), Bubbles and their role in gas exchange, in *The Sea Surface and Global Change*, vol. 10, edited by Peter S. Liss and Robert A. Duce, pp. 173–205, Cambridge University Press, Cambridge, U. K., doi:10.1017/CBO9780511525025.007.

Woolf, D. K. (2005), Parametrization of gas transfer velocities and sea-state-dependent wave breaking, *Tellus, Ser. B*, *57*(2), 87–94, doi:10.1111/j.1600-0889.2005.00139.x.

Wu, J. (1988), Variations of whitecap coverage with wind stress and water temperature, *J. Phys. Oceanogr.*, *18*(10), 1448–1453, doi:10.1175/1520-0485(1988)018⟨1448:VOWCWW⟩2.0.CO;2.

Yelland, M. J., B. I. Moat, R. W. Pascal, and D. I. Berry (2002), CFD model estimates of the airflow distortion over research ships and the impact on momentum flux measurements, *J. Atmos. Oceanic Technol.*, *19*(10), 1477–1499, doi:10.1175/1520-0426(2002)019⟨1477:CMEOTA⟩2.0.CO;2.

Yueh, S. (1997), Modeling of wind direction signals in polarimetric sea surface brightness temperatures, *IEEE Trans. Geosci. Remote Sens.*, *35*(6), 1400–1418, doi:10.1109/36.649793.

Zhao, D., and Y. Toba (2001), Dependence of whitecap coverage on wind and wind-wave properties, *J. Oceanogr.*, *57*(5), 603–616.

Žutić, V., B. Ćosović, E. Marčenko, N. Bihari, and F. Kršinić (1981), Surfactant production by marine phytoplankton, *Mar. Chem.*, *10*(6), 505–520, doi:10.1016/0304–4203(81)90004-9.